

FRIENDLY Regulates Mitochondrial Distribution, Fusion, and Quality Control in Arabidopsis¹[W][OPEN]

Amr M. El Zawily, Markus Schwarzländer, Iris Finkemeier, Iain G. Johnston, Abdelilah Benamar, Yongguo Cao, Clémence Gissot, Andreas J. Meyer, Ken Wilson, Raju Datla, David Macherel, Nick S. Jones, and David C. Logan*

Department of Biology, University of Saskatchewan, Saskatoon, Saskatchewan, Canada S7N 5E2 (A.M.E.Z., K.W., D.C.L.); Faculty of Science, Damanhour University, Damanhour 22516, Egypt (A.M.E.Z.); Institute of Crop Science and Resource Conservation, University of Bonn, D-53113 Bonn, Germany (M.S., A.J.M.); Max-Planck-Institute for Plant Breeding Research, Plant Proteomics Group, 50829 Cologne, Germany (I.F.); Department of Mathematics, Imperial College London, London SW7 2AZ, United Kingdom (I.G.J., C.G., N.S.J.); Université d'Angers, Institut National de la Recherche Agronomique, and Agrocampus Ouest, Unité Mixte de Recherche 1345, Institut de Recherche en Horticulture et Semences, Angers F-49045, France (A.B., D.M., D.C.L.); and Plant Biotechnology Institute, National Research Council of Canada, Saskatoon, Saskatchewan S7N 0W9, Canada (Y.C., R.D.)

ORCID IDs: 0000-0002-3352-2185 (D.M.); 0000-0002-8980-240X (D.C.L.).

Mitochondria are defining components of most eukaryotes. However, higher plant mitochondria differ biochemically, morphologically, and dynamically from those in other eukaryotes. *FRIENDLY*, a member of the CLUSTERED MITOCHONDRIA superfamily, is conserved among eukaryotes and is required for correct distribution of mitochondria within the cell. We sought to understand how disruption of *FRIENDLY* function in Arabidopsis (*Arabidopsis thaliana*) leads to mitochondrial clustering and the effects of this aberrant chondriome on cell and whole-plant physiology. We present evidence for a role of *FRIENDLY* in mediating intermitochondrial association, which is a necessary prelude to mitochondrial fusion. We demonstrate that disruption of mitochondrial association, motility, and chondriome structure in *friendly* affects mitochondrial quality control and leads to mitochondrial stress, cell death, and strong growth phenotypes.

Mitochondria are a defining component of eukaryotes: even the few groups of amitochondriate protists are believed to have secondarily lost the organelle (Clark and Roger, 1995; Bui et al., 1996; Gray et al., 1999). The long shared history of eukaryotes has led to considerable conservation of mitochondrial structure and function, although some divergence of both has occurred between plants, fungi, and animals since they split from their most recent common ancestor approximately 1,500 million years ago (Feng et al., 1997; Douzery et al., 2004; Hedges et al., 2004).

The higher plant chondriome (the collective term for all mitochondria in a cell; Logan, 2006) differs from the

chondriome in animal cells and in yeast in terms of motility and structural organization (Logan, 2010a). In general, animal and yeast mitochondria move on microtubules, whereas in higher plants mitochondria move on actin. The difference in cytoskeletal track used for movement may in part explain the difference in gross chondriome structure. The plant chondriome typically exists as a population of several hundred small, physically discrete organelles that interact genetically via fusion (i.e. as a discontinuous whole; Logan, 2006), while the animal chondriome, although varying according to cell type, is typically more of a reticular structure, as in yeast (Bereiter-Hahn and Vöth, 1994; Rafelski, 2013).

Chondriome structure in eukaryotes is maintained by a balance of fusion, between physically discrete parts of the chondriome, and subsequent fission. A predominance of fusion over fission, caused by genetic deletion of components of the fission apparatus, leads to a more reticular network chondriome, while genetic deletion of components of the fusion apparatus in yeast and animal cells leads to a fragmentation of the chondriome (Shaw and Nunnari, 2002; Karbowski and Youle, 2003; Okamoto and Shaw, 2005; Hoppins and Nunnari, 2009). It is clear that disruption of mitochondrial fission in plants leads to the production of long, reticular mitochondria (Arimura and Tsutsumi, 2002; Logan et al., 2003, 2004; Scott et al., 2006). However, we know nothing of the plant fusion apparatus.

¹ This work was supported by the Natural Sciences and Engineering Research of Canada (Discovery Grant to D.C.L.), the Canada Foundation for Innovation, the University of Saskatchewan, the Biotechnology and Biological Sciences Research Council of the United Kingdom (grant no. BB/C000129/1), the University of Angers, the Campus Vegetal project through Qualité et Santé du Végétal, and the Deutsch Forschungsgemeinschaft (Emmy-Noether Programme grant no. SCHW 1719/1-1 to M.S.).

* Address correspondence to david.logan@univ-angers.fr.

The author responsible for distribution of materials integral to the findings presented in this article in accordance with the policy described in the Instructions for Authors (www.plantphysiol.org) is: David C. Logan (david.logan@univ-angers.fr).

[W] The online version of this article contains Web-only data.

[OPEN] Articles can be viewed online without a subscription.

www.plantphysiol.org/cgi/doi/10.1104/pp.114.243824

The fundamental differences in the structure of plant and nonplant chondriomes and the lack of conservation of genes, identified to date, as involved in mitochondrial fusion (Logan, 2003, 2010b) led one of us to perform a microscopy-based screen to identify *Arabidopsis thaliana* mutants with disrupted chondriome structure with the goal of discovering genes involved in plant mitochondrial fusion and plant-specific genes involved in plant mitochondrial fission (Logan et al., 2003). One of the mutants, called *friendly* (or *friendly mitochondria*), was identified due to the presence of large clusters of mitochondria rather than the homogenous distribution of mitochondria in the wild type (Logan et al., 2003). *FRIENDLY* (At3g52140) was identified by a combination of map-based cloning and candidate gene sequencing, and the mutant null allele contains a single G-to-A nucleotide mutation destroying the second exon-intron consensus motif (Logan et al., 2003). *FRIENDLY* is a member of the CLUSTERED MITOCHONDRIA (CLU) superfamily of conserved eukaryotic proteins (National Center for Biotechnology Information Conserved Domains Database accession no. cl16180), but despite encoding a protein with a molecular mass of approximately 150 kD, there are no clues to protein function in its sequence. Here, we set out to understand how disruption of *FRIENDLY* function leads to the clustered mitochondrial phenotype and the effects of this aberrant chondriome on cell and whole-plant physiology.

We present empirical cell biological and theoretical mathematical evidence that the mechanism responsible for the *friendly* mutant phenotype is an extended duration of intermitochondrial association, which is a necessary prelude to intermitochondrial fusion. We demonstrate that disruption of normal mitochondrial association and chondriome structure has negative effects on cell and whole-organism health, including mitochondrial stress, cell death, and modifications to whole-organism growth.

RESULTS

Mitochondria in *friendly* Are Organized into Large Clusters

The *friendly* mutant was originally identified (Logan et al., 2003) due to the clustered mitochondrial phenotype; however, no analysis was made regarding the size distribution of clusters relative to the wild type. Here, mitochondria in wild-type plants were found to be distributed evenly throughout the cytoplasm in both leaves and roots, while in *friendly*, many mitochondria were arranged in large clusters of tens of organelles in addition to singletons that had a distribution resembling the wild type (Fig. 1A; Supplemental Movie S1). In order to quantify cluster number and size, clusters were defined as discrete associations in an area of at least $2.5 \mu\text{m}^2$ (see "Materials and Methods"), a phenotype that was not observed in healthy wild-type plants. While no clusters were observed in the wild type, some mitochondria were observed to be in loose groups with an average area of $0.41 \mu\text{m}^2$ in leaf epidermal pavement cells and $0.79 \mu\text{m}^2$

in root epidermal cells (Fig. 1B). The average mitochondrial cluster size in *friendly* leaf epidermal pavement cells was $9.7 \mu\text{m}^2$, while significantly larger clusters covering an average of $16.09 \mu\text{m}^2$ were observed in roots (Fig. 1C). There was no significant difference in the number of clusters in leaves or roots in *friendly* (Fig. 1C). The majority of groups in the wild type covered an area less than $0.5 \mu\text{m}^2$ in both leaves and roots, while the larger size classes were more frequently observed in root cells, reflecting the greater mean group size in this cell type (Fig. 1, compare D and E). In *friendly*, the majority of clusters fell within the 2.5 - to 10 - μm^2 range, while, as in the wild type, clusters covering larger areas were more frequently present in roots than in leaves (Fig. 1E). A similar phenotype was observed in the *friendly-3* transfer DNA (T-DNA) mutant (Supplemental Fig. S1).

Clusters in the *friendly* Mutant Are Composed of Discrete Organelles

Mitochondrial clusters in leaves prepared for transmission electron microscopy (TEM) by chemical fixation showed no obvious outer membrane connectivity (Logan et al., 2003). However, given the importance of any intermitochondrial connection in the mutant to the role of *FRIENDLY*, we decided to investigate this further by two complementary methods. In order to determine whether or not mitochondria in clusters in *friendly* were connected to each other by a contiguous outer membrane, leaf material prepared by high-pressure freezing was viewed by TEM. Membranous structures were well preserved within the cytoplasm of both wild-type and mutant leaves (Fig. 2A), allowing clear identification of fine membranous organelles such as the Golgi and endoplasmic reticulum (ER) and thylakoids within chloroplasts. No organelles other than mitochondria appeared to be affected, morphologically, by the *friendly* mutation. Over 40 ultrathin sections were observed from at least three plants, and there was no evidence of continuity of the outer membrane between mitochondria in a cluster. However, electron-dense regions were observed between individual mitochondria within a cluster (Fig. 2, A and B, arrows).

An independent approach was used to investigate the connectivity of the mitochondrial matrices of adjacent mitochondria in a cluster using fluorescence recovery after photobleaching (FRAP) of the mitochondrial-targeted (mito)-GFP fluorescence. A strip through a cluster was photobleached using the 488-nm laser, and no recovery was observed up to 300 s after bleaching (Fig. 2C; Supplemental Movie S2). Due to the physically dispersed nature of the wild-type *Arabidopsis* chondriome, a meaningful photobleaching control could not be performed on the wild type. Instead, in order to observe how quickly GFP could diffuse within a mitochondrion (as a proxy for contiguous matrices within a cluster), we performed FRAP on mitochondrial tubules of the *network* mutant first identified by Logan et al. (2003). mito-GFP was able to diffuse into bleached areas of the matrix within 1.5 s (Fig. 2D; Supplemental Movie S2).

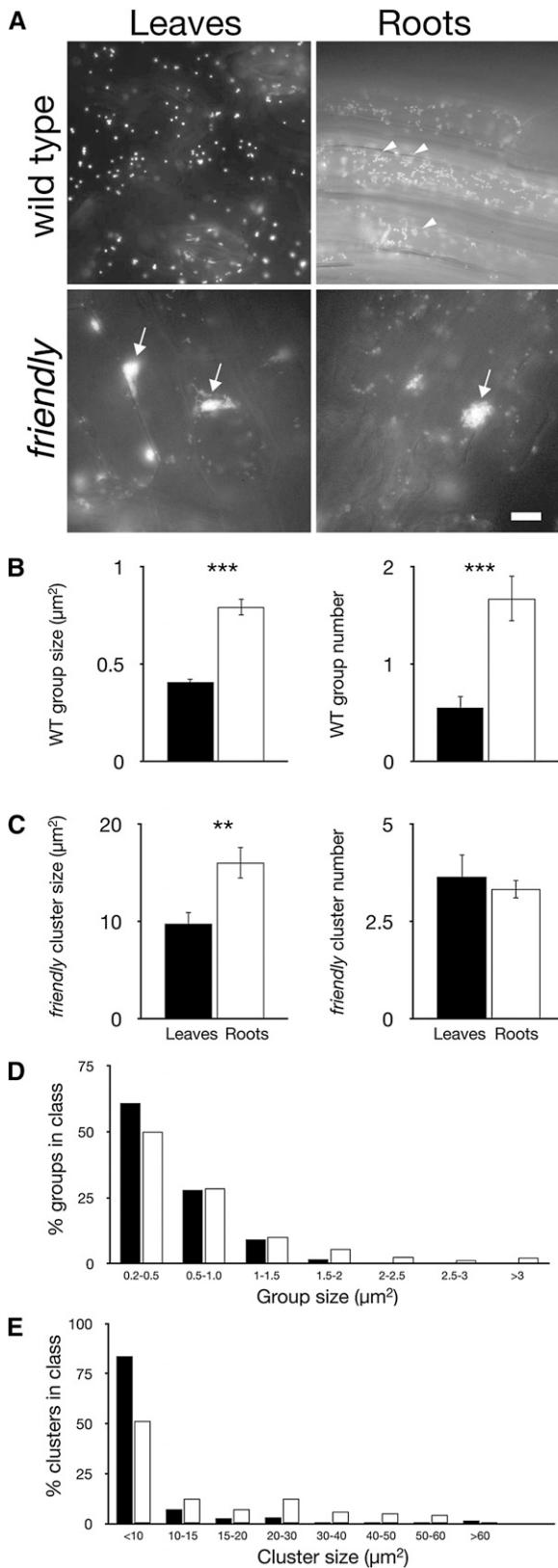


Figure 1. The *friendly* mutant is characterized by the presence of large clusters of mitochondria. A, Epifluorescence micrographs of root and leaf cells of 7-d-old *Arabidopsis* seedlings of the *friendly* mutant and its

Mitochondria in *friendly* Move on F-Actin, and Clusters Can Be Disrupted by Restructuring of the F-Actin Cytoskeleton

We next focused on the dynamism of clusters in *friendly* and their interaction with the cytoskeleton. Single mitochondria in *friendly* move on actin filaments as in the wild type (Supplemental Movie S3). Similarly, small clusters of mitochondria in *friendly* are also able to move on actin filaments (Fig. 3A; Supplemental Movie S3), and depolymerization of F-actin with latrunculin B arrests this movement (Supplemental Movie S3). Larger clusters assemble due to the aggregation of smaller clusters that are brought together through movement on actin, and these large clusters are less able to move through the cytosol intact and are disrupted by the forces of cytoplasmic streaming, such as restructuring of the actin cytoskeleton and physical bottlenecks in the cytoplasm (Fig. 3B; Supplemental Movies S4 and S5). Clusters of mitochondria in *friendly*, therefore, are highly dynamic transient structures composed of discrete organelles that are able to interact with the actin cytoskeleton in a wild-type manner. Furthermore, while we had previously hypothesized that clusters in *friendly* may be tethered to microtubules, we found no evidence of any association with either microtubules themselves (Supplemental Movie S6; Sampathkumar et al., 2011) or more specifically the plus-ends of microtubules (Supplemental Movie S6), and partial depolymerization of microtubules did not affect the movement of clusters (Supplemental Movie S6). In contrast, depolymerization of the actin cytoskeleton in the wild type using latrunculin B was able to phenocopy the *friendly* phenotype (Supplemental Fig. S2A). This apparent stickiness of mitochondria in the absence of their actin scaffold is not observed with other organelles that move on actin. For example, while peroxisomes and Golgi bodies move on actin and latrunculin B arrests this movement, neither organelle forms large clusters in response to actin depolymerization (Nebenführ et al., 1999; Brandizzi et al., 2002; Mano et al., 2002; Mathur et al., 2002; Sparkes et al., 2008). Furthermore, the clustering of mitochondria in *friendly* is not due to a general cytoskeletal or motor defect, since the distribution and movement of peroxisomes are not affected in the mutant (Supplemental Fig. S2B), and no altered distribution of other organelles was observed in TEM images (Fig. 2, A and B).

These observations support the hypothesis that mitochondria are attracted to one another and that movement

wild type (mito-GFP). Arrowheads indicate groups of mitochondria in the wild type, and arrows indicate clusters. Bar = 10 μm . B, Group size and number in the wild type (WT). C, Cluster size and number in *friendly*. Values in B and C are averages calculated from 40 pairs of images of leaf (black bars) or root (white bars) epidermal cells, and each of the 40 pairs of images was of a separate plant. Error bars indicate SE ($n = 40$). D and E, Frequency distribution of group sizes in the wild type and cluster size in *friendly*, respectively. Black bars represent values from leaves, and white bars represent values from roots. ** $P \leq 0.01$, *** $P \leq 0.001$.

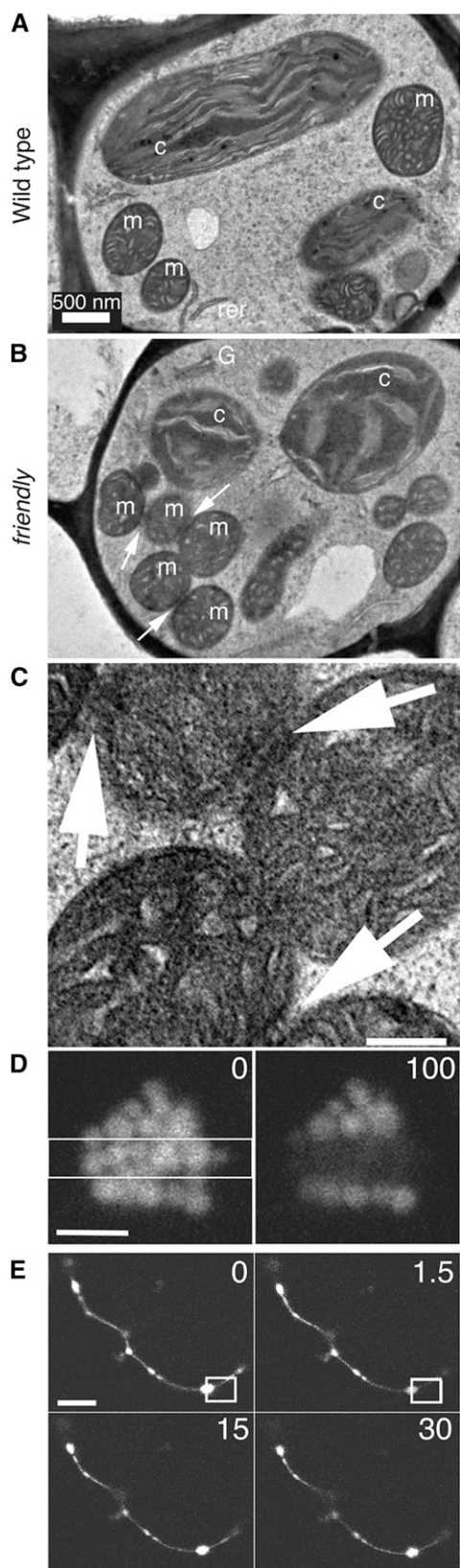


Figure 2. Clusters in the *friendly* mutant are discrete organelles. A and B, Mesophyll cells in high-pressure frozen sections of Arabidopsis leaf of the wild type (A) and *friendly* (B) at the same magnification. c, c,

on actin filaments counters this attraction by providing the scaffold and driving force to keep mitochondria separate except during their regulated association and transient fusion.

FRIENDLY Is a Cytosolic Protein with Either a Diffuse Expression Pattern or a Speckled Pattern Associated with Mitochondria

A C-terminal translational fusion of GFP to the full-length *FRIENDLY* complementary DNA (cDNA) coding sequence was generated to visualize the *FRIENDLY* location. Expression of *FRIENDLY*-GFP in wild-type Arabidopsis showed a cytosolic location, often with a punctate distribution (Fig. 4, A and B). Similar localization patterns were observed using transient expression in tobacco (*Nicotiana tabacum*; Fig. 4, C–E). To demonstrate that this expression pattern was unlikely to be due to overexpression, we performed transient expression in *friendly* seedlings: both C- and N-terminal fusions to monomeric Red Fluorescent Protein1 (mRFP1) showed a punctate distribution in close association with mitochondria (Supplemental Fig. S3). Cotransformation of tobacco with *FRIENDLY*-GFP and mito-mCherry demonstrated that the *FRIENDLY*-GFP puncta were frequently associated with mitochondria (Fig. 4C). That this was a dynamic association is evident from the time-lapse movie (Supplemental Movie S7). As with stable transformation in Arabidopsis, a punctate pattern was not always observed; instead, a more diffuse cytoplasmic distribution was apparent (Fig. 4D). In the cortical cytoplasm, this appeared as a reticulum, as the fusion protein was excluded from areas occupied by other organelles (Fig. 4E). In order to exclude the possibility that *FRIENDLY*-GFP was localized to organelles exhibiting a similar punctate pattern, coexpression in tobacco was performed with fluorescent markers of peroxisomes (mCherry-peroxisome targeting signal1 [PTS1]; Fig. 4F) and the Golgi (sia1 transferase [ST]-mRFP1; Fig. 4G): no colocalization was apparent. Similarly, the cortical reticular pattern of *FRIENDLY*-GFP was distinct from that of the ER visualized by coexpression of the ER marker er-RB (Fig. 4H). Our data demonstrating a cytosolic localization is in agreement with a recent cytosol proteomic study (Ito et al., 2011). The yeast *FRIENDLY* ortholog, CLU1, also has been localized by proteomics to the cytosol (Kumar et al., 2002), and the *Drosophila melanogaster* ortholog, Clu, has been shown to be a cytosolic protein

Chloroplast; G, Golgi apparatus; m, mitochondrion; rer, rough ER. C, Higher magnification TEM scan of the cluster in B. Arrows in B and C indicate electron-dense regions between mitochondria. D, FRAP of a cluster in *friendly*. At left is the cluster prebleach and at right is the cluster 100 s postbleach (Supplemental Movie S2). E, FRAP of a long mitochondrial tubule in the *network* mutant. At top left is the tubule prebleach, and the other images show the same view 1.5, 15, and 30 s postbleach (Supplemental Movie S2). Bars = 200 nm in C and 10 μ m in D and E.

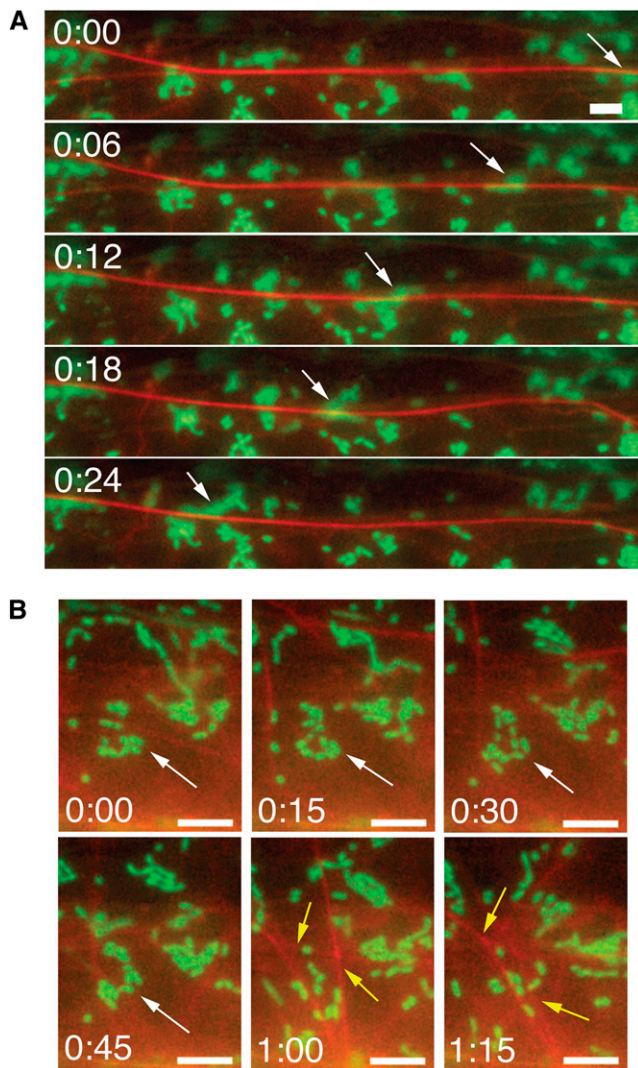


Figure 3. Mitochondria in *friendly* move on the actin cytoskeleton, and clusters are disrupted by the dynamic actin cytoskeleton. Mitochondria are visualized by mito-GFP fluorescence and actin by mCherry-mTalin. A, Single images from a time-lapse movie showing a small cluster of mitochondria (arrows) moving on actin (Supplemental Movie S3). B, Single images from a time-lapse movie showing a cluster developing (white arrows) up to 60 s, when it is disrupted by rearrangement of the actin cytoskeleton (yellow arrows; Supplemental Movie S5). Bars = 5 μ m.

that associates peripherally with mitochondria in *D. melanogaster* follicle nurse cells (Cox and Spradling, 2009).

Clusters in *friendly* Form Due to an Increase in the Time of Association between Mitochondria That Meet through the Movement on Actin

Our observations of the movement of mitochondrial clusters on actin, the role of actin in bringing mitochondria together in the formation of clusters, and the dynamism of clusters led us to consider how clusters

form. Mitochondria in wild-type *Arabidopsis* that meet one another through the movement on actin often display a short period of association (Fig. 5A) during which time fusion and subsequent fission can occur, a phenomenon also seen in some mammalian cells and termed “kiss and run” (Twig et al., 2008). Figure 5A displays individual frames from Supplemental Movie S8 that show two association/disassociation events in the wild type: the images reference one of these associations that occurs within 20 s (at 19 s in the movie) and the subsequent disassociation that occurs within a further 10 s (at 28 s in the movie). In contrast, the images in Figure 5B reference an association/disassociation event between an initially discrete single mitochondrion and another mitochondrion at the exterior of a cluster in *friendly* (Supplemental Movie S8): the single mitochondrion associates with the cluster within 20 s (at 18 s in the movie) and disassociates 62 s later. By analyzing 45 movies each of the wild type and *friendly*, we were able to quantify the average length of intermitochondrial association: in the wild type, the average is 15 ± 0.7 s (Fig. 5C); however, in the *friendly* mutant, the average time of association is significantly greater at 61.5 ± 1.4 s (Fig. 5C). This extended association time between mitochondria in *friendly* is sufficient to lead to the buildup of a cluster as more mitochondria become temporarily associated before eventually being able to leave the cluster if sufficiently close to a filament of actin (Fig. 3B; Supplemental Movie S3).

To demonstrate that longer association times lead to more mitochondrial clustering, we constructed and simulated a simple stochastic model of mitochondrial dynamics (see “Materials and Methods”). In this model, mitochondria, represented as individual agents, undergo random motion on a three-dimensional lattice, with the rate of mitochondrial motion depending on whether a mitochondrion is clustered (adjacent to other mitochondria) or free. As mean association time increases, the proportion of mitochondria existing in clusters in the steady state increases in concert (Fig. 5D; Supplemental Movie S8). This provides independent theoretical evidence that alteration of mitochondrial association alone could be responsible for the clustering of mitochondria in *friendly*. In Supplemental Document S1, we also provide a simple analytic argument that qualitatively recapitulates this behavior.

The Frequency of Mitochondrial Membrane Potential Pulsing Is Increased in *friendly*

It was suggested recently that mitochondrial fusion involves the formation of a pore in the inner mitochondrial membrane, thereby causing transient changes in the membrane potential of the fusion partners (Santo-Domingo et al., 2013). We decided, therefore, to investigate membrane potential dynamics in *friendly*. Transient changes in membrane potential, which we term pulses (Schwarzländer et al., 2012b), are rare events in the wild type; thus, it was immediately evident from confocal

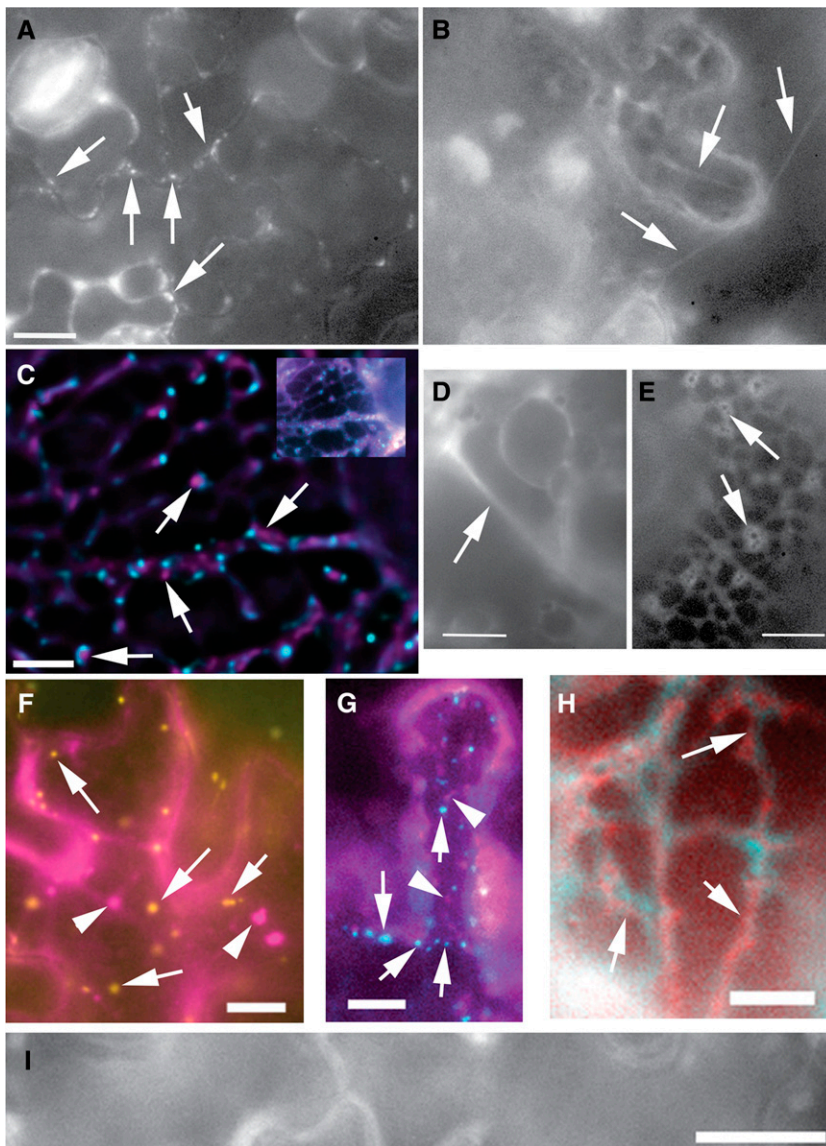


Figure 4. FRIENDLY displays a diffuse cytosolic location but sometimes also organizes into puncta. A, Localization of FRIENDLY-GFP to discrete puncta (indicated by arrows) in epidermal pavement cells of stable transformed wild-type Arabidopsis. Bar = 10 μ m. B, Diffuse localization of FRIENDLY-GFP in the cytosol of stable transformed wild-type Arabidopsis. Arrows indicate transvacuolar cytoplasmic strands. The scale is as in A. C, Localization of FRIENDLY-GFP (magenta) and mito-mCherry (cyan) by transient expression in tobacco leaf epidermal pavement cells. Arrows indicate FRIENDLY-GFP puncta. The image has been subjected to deconvolution using AutoDeblur, and the original processed image is shown in the inset (Supplemental Movie S7). Bar = 5 μ m. D and E, Localization of FRIENDLY-GFP by transient expression in tobacco leaf epidermal pavement cells. The arrow in D indicates transvacuolar cytoplasmic strands. The cortical layer of a cell is imaged in E, and the arrows indicate negatively stained organelles. F to H, Cotransformation of FRIENDLY-GFP and various organelle markers by transient transformation in tobacco, as for C to E. F, Peroxisomes (arrows = mCherry-PTS1; yellow) and FRIENDLY-GFP (arrowheads = puncta; magenta). G, Golgi ST-RFP (arrows; cyan) and FRIENDLY-GFP (arrowheads = puncta; magenta). H, ER marker er-RB (cyan) and FRIENDLY-GFP (red). Arrows indicate regions where the two colors are clearly not coincident. I, Control tobacco leaf epidermis infiltrated with buffer only. Bars in D to I = 10 μ m.

scanning laser microscopy (CSLM) imaging that the number of mitochondria exhibiting pulses and the frequency of pulses were greater in *friendly* than in the wild type (Fig. 6A). Mitochondria undergoing a pulse in the reference images of hypocotyl cells expressing mito-GFP (Fig. 6A; Supplemental Movie S9) are identified by their green color, due to mito-GFP fluorescence in the absence of the matrix-localized red tetramethylrhodamine, methyl ester (TMRM), while mitochondria with a greater membrane potential are yellow-orange, due to the colocalization of TMRM and mito-GFP in their matrices. In *friendly*, the extent of pulsing was highly variable between cells and there was considerable heterogeneity of membrane potential within the chondriome, although in general mitochondria in clusters showed the same baseline membrane potential as those not in clusters (Fig. 6A). Quantification of the number of pulses showed that the average frequency of pulses was 0.12 per 100

mitochondria per minute in the wild type, while in *friendly* it was increased to 11.14 per 100 mitochondria per minute, an increase of approximately 100 \times (Fig. 6B). There was no significant difference in the frequency of pulses for mitochondria in a cluster (mean = 9.82, 95% confidence interval [4.08, 18.03]) compared with those not in clusters (mean = 12.29, 95% confidence interval [5.65, 21.48]). Our interpretation of these results is that fusion initiation events, via the formation of a fusion pore, occur with higher frequency in *friendly* relative to the wild type.

An in Vivo Fusion Assay Demonstrates That Matrix Mixing Is Increased in *friendly*

To test whether the increased rate of pulsing correlated with an increase in the extent of matrix mixing, and therefore intermitochondrial fusion, we devised a

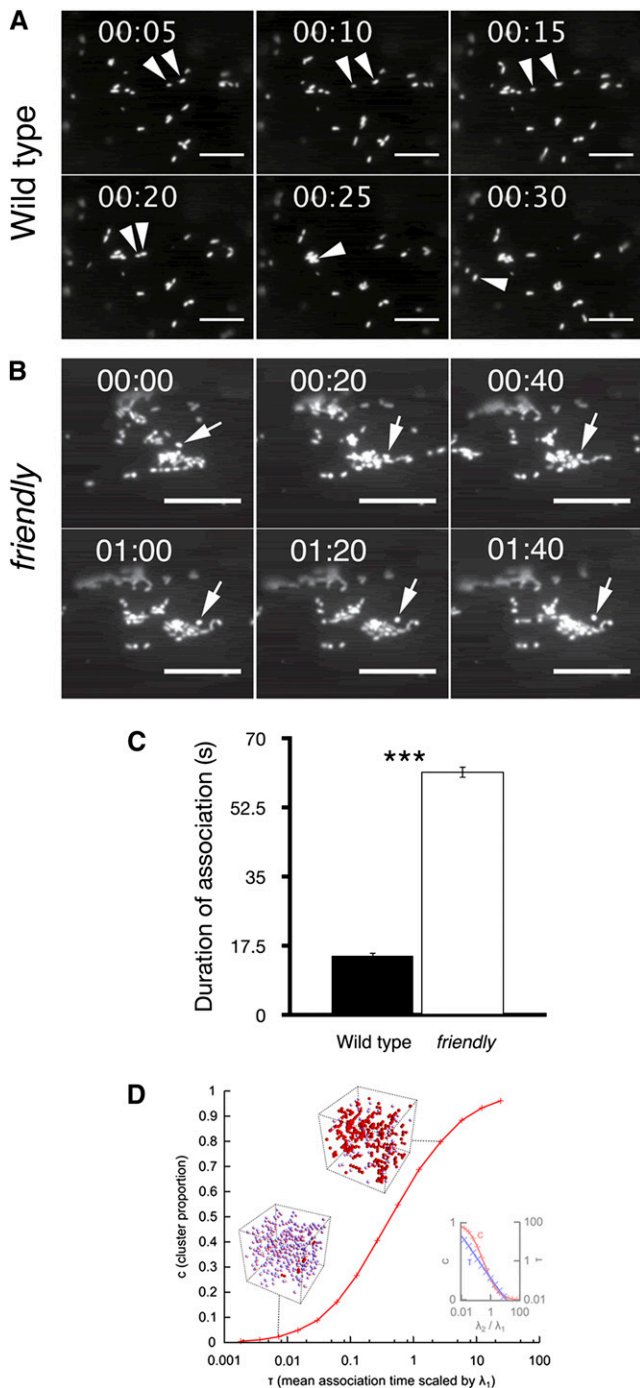


Figure 5. Association time between mitochondria in the wild type and the *friendly* mutant. **A**, Images show single frames from a movie (Supplemental Movie S8) of mitochondria in a wild-type leaf epidermal pavement cell in which two mitochondria meet by 20 s (arrowheads; 19 s in the movie) and separate by 30 s (28 s in the movie). **B**, Images show single frames of mitochondria in leaf epidermal pavement cell from the *friendly* mutant in which a mitochondrion (arrow) joins a cluster at 18 s and then separates from the cluster at 1 min, 20 s (Supplemental Movie S8). Bars = 10 μ m. **C**, Quantification of the duration, in seconds, of the association of single mitochondria in the wild type (black bar) or a mitochondrion and a cluster in *friendly* (white bar). Values represent the mean duration calculated from three independent experiments ($n = 3$)

quantitative in vivo fusion assay using the mitochondria-targeted photoconvertible protein mito-monomeric (m)Eos (Mathur et al., 2010). Matrix-localized mEos was photoconverted within highly motile mitochondria in a region of leaf epidermis (Fig. 6C; Supplemental Movie S10). The percentage reduction in numbers of green mitochondria, as a result of the exchange of matrix contents during repeated transient fusion events with mitochondria containing photoconverted mEos, was significantly greater at the end of the assay time period in *friendly* (30.4%) relative to that in the wild type (14.2%; Fig. 6D). The fact that an exchange of matrix contents was not seen in the FRAP experiments can likely be accounted for simply because we analyzed, by necessity, a single relatively immobile cluster by photobleaching and, therefore, interaction with other mitochondria outside of the cluster could not occur. Similarly, the fusion assay, by necessity, required mitochondria to be motile, since there would be no fusion between dispersed mitochondria unless they were able to meet. In addition, observation of hundreds of individual association events between a single red mitochondrion and a single green mitochondrion failed to demonstrate extensive mixing of the two mEos species, suggesting that there is limited matrix exchange per fusion event, as reported for mammalian cells (Huang et al., 2013; Santo-Domingo et al., 2013).

The result of this fusion assay demonstrates that the increased association time is not simply due to mitochondria trying but failing to fuse with one another but that it increases the chance that transient fusion events can occur, facilitating the exchange of matrix content.

The Mitochondrial Phenotype in *friendly* Is Associated with Defective Whole-Plant Phenotypes, Including Lower Biomass, Shorter Roots, and Shorter Etiolated Hypocotyls

While *friendly* was identified solely on the basis of its mitochondrial phenotype, there is a series of whole-plant defective phenotypes as a consequence. Plants of the same age are smaller and have shorter, more rounded leaves (Fig. 7A). Biomass is reduced in *friendly*, significantly so at 7 to 21 d old (Fig. 7B); however, the most obvious phenotypic difference between the mutant

of individual mitochondrial associations calculated from movies of five cells in each of three plants per experiment (15 movies per experiment). Error bars indicate SE. *** $P \leq 0.001$. **D**, Stochastic modeling demonstrates that increased association time between mitochondria leads to increased cluster formation. The proportion of model mitochondria in a stochastic simulation (see “Materials and Methods”) existing as part of a cluster, as the mean association time between adjacent mitochondria varies, is shown. To obtain this relationship, λ_1 , the diffusion rate of free mitochondria, is fixed to define unit time, and λ_2 , the diffusion rate of clustered mitochondria, is varied. The inset plot shows how clustered proportion and mean association time vary with λ_2 . If mitochondria are very sticky, then λ_2/λ_1 will be much less than 1. Inset images show example snapshots (with periodic boundary conditions) of the stochastic model at the given association times; clustered mitochondria are shown in dark red.

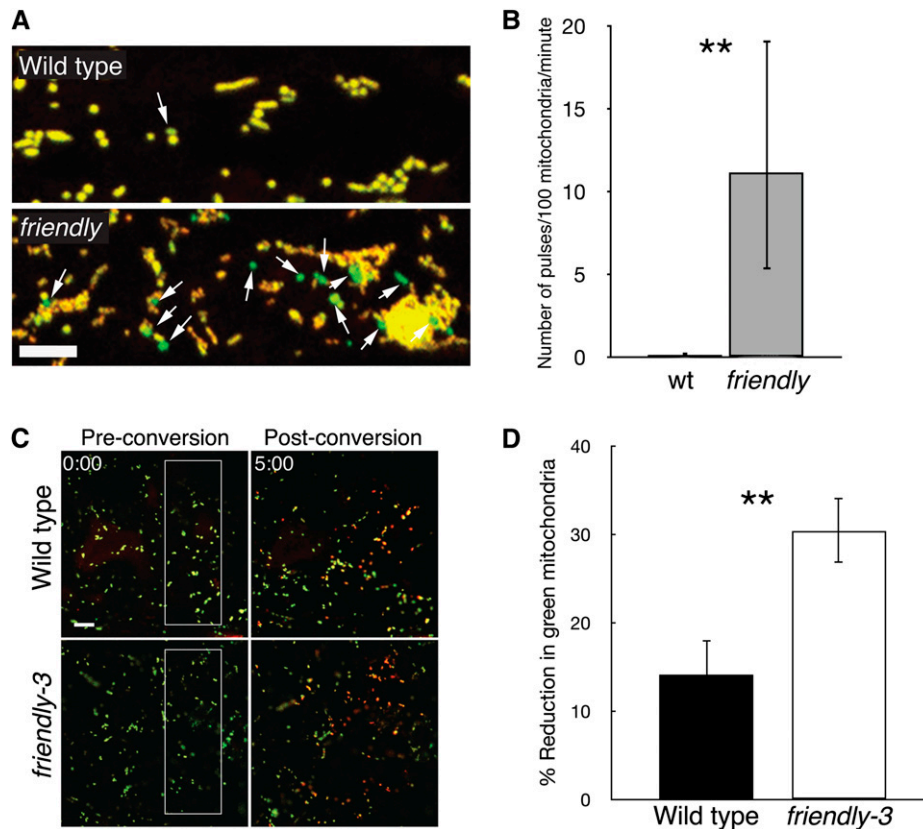


Figure 6. The frequencies of mitochondrial membrane potential pulsing and matrix mixing are increased in *friendly*. **A**, Representative images of mitochondria in control (wild-type mito-GFP) and *friendly* hypocotyl cells stained with 50 nM TMRM. The images are merged composites of green (GFP) and red (TMRM) channels (Supplemental Movie S9). Arrows indicate mitochondria undergoing a transiently depolarizing pulse. Bar = 5 μ m. **B**, Quantification of the number of pulses per 100 mitochondria in root epidermal cells per minute. A total of 219 mitochondria were scored on average for each biological replicate. Means and 95% confidence limits are shown as error bars after back transforming from a square root transformation (** $P < 0.01$, $n = 7$ [the wild type] and $n = 6$ [*friendly*]). **C**, In vivo mitochondrial fusion assay in Arabidopsis leaf epidermal pavement cells using mitochondrially targeted mEos (mito-mEos) photoconvertible protein. These images were created by merging the red and green channels of single optical slices of leaves of the wild type or the *friendly-3* mutant stably transformed with mito-mEos. The left images show the preconverted state at time zero, and the outlined boxes indicate the region subjected to photoconversion. Images were captured continuously at 1/4 fps until 5 min from the start of the experiment. The right images show the last single-slice images captured at the end of the experiment (Supplemental Movie S10). Bar = 10 μ m. **D**, Quantification of the percentage reduction in the average number of green mitochondria per field of view (the whole frames as shown in C). Error bars indicate SE ($n = 8$, ** $P < 0.01$).

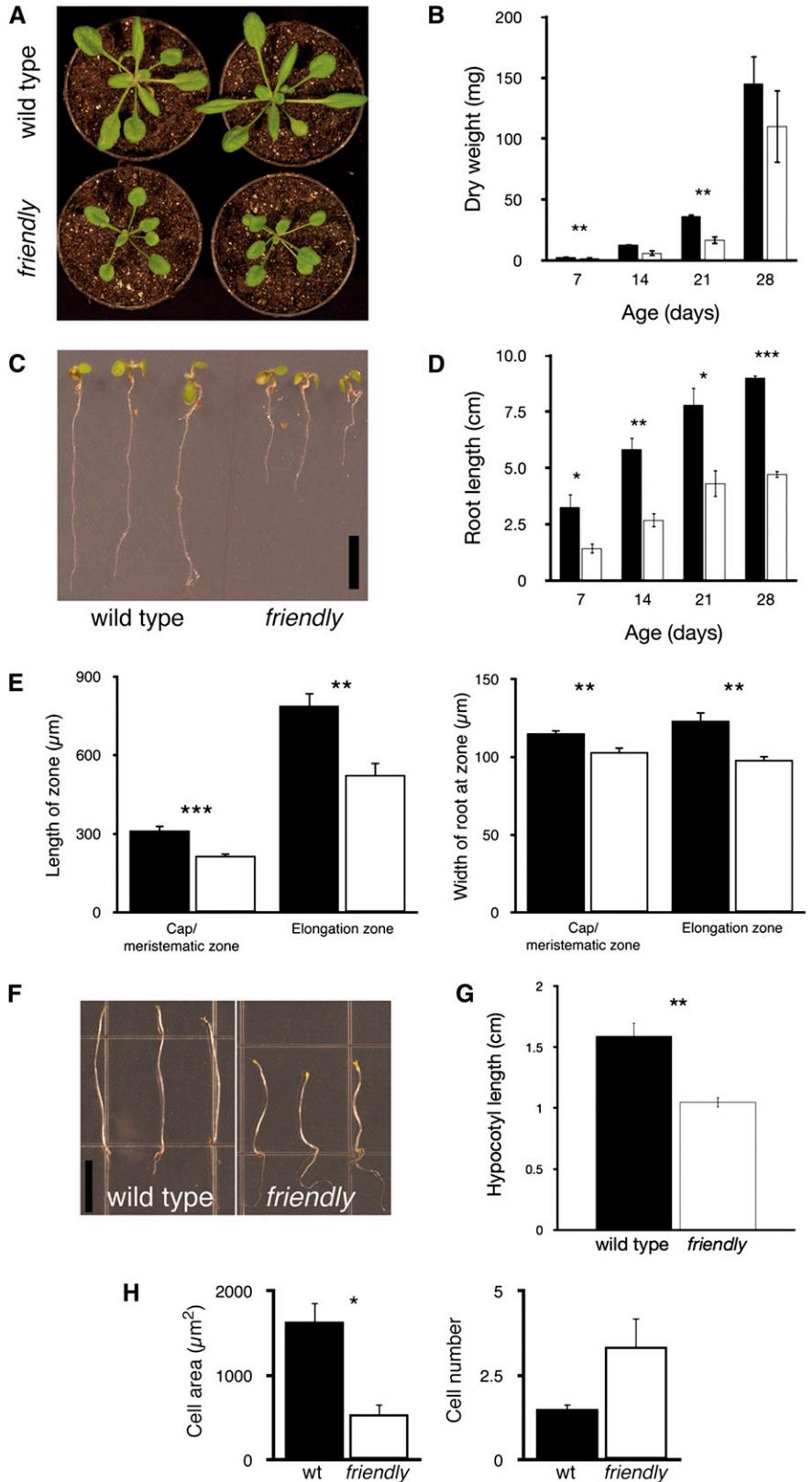
and the wild type is the length of the primary root (Fig. 7, C and D). Primary root length is significantly shorter in *friendly* seedlings at 7, 14, 21, and 28 d (Fig. 7D), such that by 28 d the root of the mutant is almost half the length of the wild type (4.72 ± 0.16 versus 9 ± 0.11 cm). Similarly, when seedlings are grown in darkness, the hypocotyl length is significantly shorter in *friendly* than in the wild type (Fig. 7, F and G). The reduction in total root length (Fig. 7, C and D) is reflected in a significant reduction in the length of the cap/meristematic region (in *friendly*, this zone is 69% the length of the zone in the wild type; Fig. 7E) and a slightly greater reduction in the elongation zone (in *friendly*, this zone is 67% of the length of the zone in the wild type; Fig. 7E). Root width was also reduced significantly in *friendly* compared with its wild type (Fig. 7E). Similar whole-plant phenotypes were

apparent in the *friendly-3* T-DNA mutant (Supplemental Fig. S4).

The Roots of *friendly* Contain Significantly Greater Numbers of Dead Cells

Propidium iodide (PI) staining of roots was performed to visualize root cell architecture in order to determine whether it was a reduction in cell number and/or cell size that was responsible for the reduction in root length. As can be seen from the data in Figure 7H, the roots of *friendly* are composed of smaller cells; therefore, there are a greater number of cells in a defined length of root tissue. However, PI staining also revealed that roots of *friendly* contained many dead cells, which are permeable to PI, while few dead cells

Figure 7. Whole-plant phenotype of the wild type and the *friendly* mutant. **A**, Rosettes in mutant and wild-type plants. **B**, Dry weight of the wild type and mutant at 7, 14, 21, and 28 d after the onset of germination. Values represent means of three independent experiments each using 15 plants; error bars indicate SE ($n = 3$). **C**, Root length of 7-d-old wild-type and mutant plants. Bar = 0.5 cm. **D**, Quantification of root length at 7, 14, 21, and 28 d after the onset of germination. Values represent means of three independent experiments each using 20 plants; error bars indicate SE ($n = 3$). **E**, Length and widths of cap/meristematic or elongation developmental zones. Values represent mean measurements from six plants; error bars indicate SE ($n = 6$). **F**, Dark-grown, etiolated seedlings after 7 d of growth in the dark. **G**, Quantification of hypocotyl length of dark-grown, etiolated seedlings 7 d after the onset of germination. Values represent means of three independent experiments each using 20 plants; error bars indicate SE ($n = 3$). **H**, Cell area and number of root epidermal cells per fixed length in the elongation zone of 6-d-old seedlings. Values represent mean measurements from four cells from each of three plants; error bars indicate SE ($n = 3$). * $P \leq 0.05$, ** $P \leq 0.01$, *** $P \leq 0.001$.



were observed in wild-type roots (Fig. 8A). For independent confirmation using a more specific and robust probe, SYTOX Orange was used as a probe that readily and selectively enters cells with a damaged plasma membrane and stains DNA. A greater number of dead cells were observed in *friendly* than in the wild type in all developmental zones (e.g. elongation zone; Fig. 8B), with significant increases measured in the elongation and differentiation zones (Fig. 8C).

The Size and Number of LysoTracker-Stained Acidic Compartments Are Increased in *friendly*

The significant increase in root cell death led us to investigate a potential breakdown in the mitochondrial quality control process in *friendly*. LysoTracker has been used to assess autophagy in plants, and while not

specific for autophagosomes, it does label acid vacuoles required for the process (Yoshimoto, 2012). We stained 6-d-old wild-type and *friendly* seedlings using 1 μM LysoTracker Red DND-99 for 5 min followed by capture of z-stacks by CSLM of the root elongation zone. We observed increases in both the size and number of LysoTracker-stained compartments in *friendly* compared with the wild type (Fig. 8D). Quantification of LysoTracker-stained compartments demonstrated that there were significant increases in the number (54 ± 8.6 in *friendly* compared with 19 ± 3.6 in the wild type) and area ($9.2 \pm 1.2 \mu\text{m}^2$ in *friendly* compared with $3.7 \pm 0.8 \mu\text{m}^2$ in the wild type) of LysoTracker-stained compartments in roots of *friendly* compared with the wild type (Fig. 8E). The increased size and number of acid compartments in *friendly* are consistent with a role for FRIENDLY in the maintenance of cell health. To

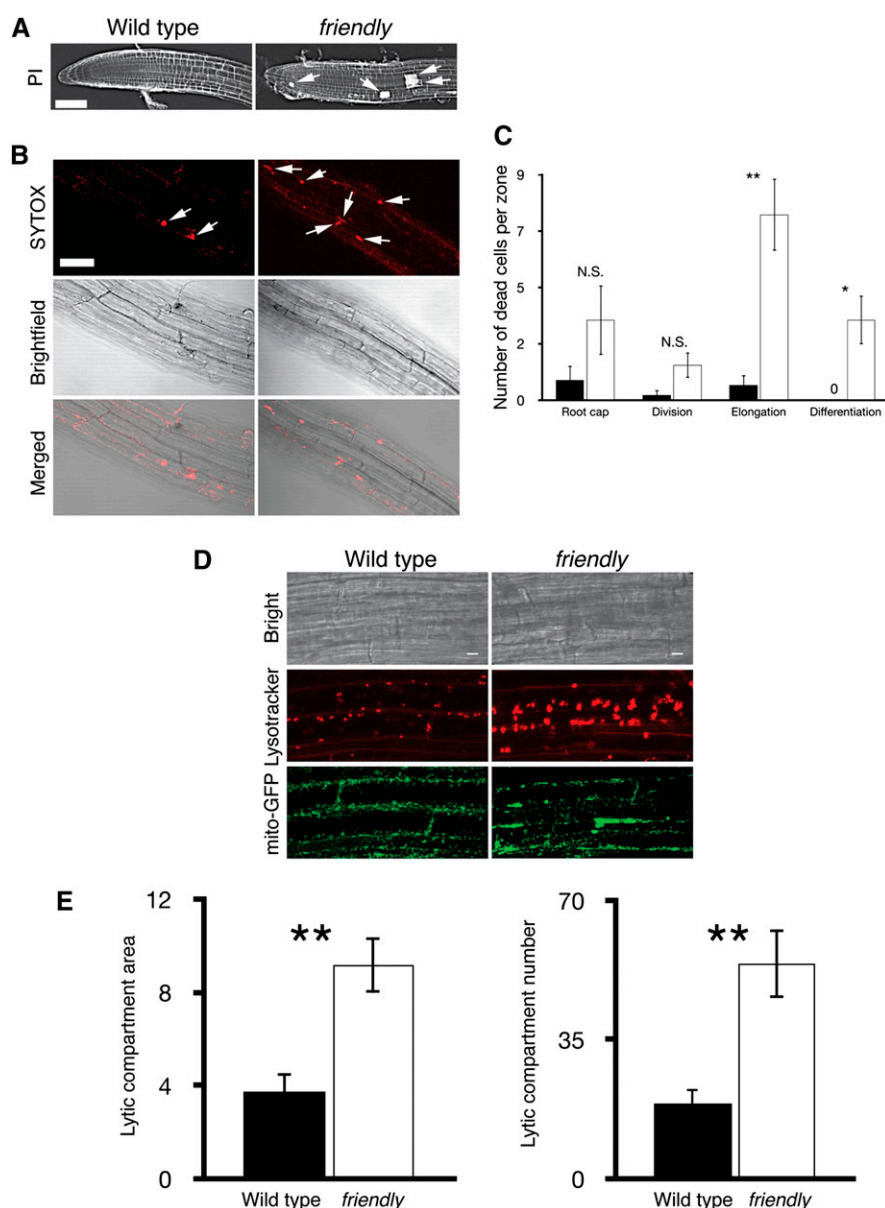


Figure 8. There are more dead cells and the size and number of LysoTracker-stained acidic compartments are increased in the roots of *friendly*. **A**, Confocal z-projections of roots of the wild type and the *friendly* mutant after staining with PI. Arrows indicate dead cells identified by the entry of PI into the cell. Bar = 100 μm . **B**, Identification of dead cells (arrows) in wild-type and *friendly* roots using SYTOX Orange. The top row shows confocal z-projections of the red, SYTOX Orange channel, the middle row shows the bright field channel, and the bottom row shows the merged SYTOX Orange and bright-field channels. Bar = 50 μm . **C**, Quantification of the number of cells in each zone of the roots of the wild type (black bars) and *friendly* (white bars). Dead cells were identified by the presence of a SYTOX Orange-stained nucleus. Values represent mean numbers of dead cells in five plants; error bars indicate SE ($n = 5$). * $P \leq 0.05$, ** $P \leq 0.01$. **D**, Representative maximum projections of 16 1- μm optical sections through the epidermal cells of the root elongation zone: bright field, LysoTracker-stained compartments, and mitochondria. Bars = 10 μm . **E**, Quantification of the area and number of LysoTracker-stained compartments in roots imaged as in **A** using the Analyze Particles option in Image J. Error bars indicate SE (** $P < 0.01$, $n = 5$).

discover what other processes and functions are altered in *friendly* that may contribute to the loss of cell health and the whole-plant phenotypes, we decided to analyze the *friendly* transcriptome.

***friendly* Shows Global Transcriptome Reprogramming Indicating Mitochondrial Dysfunction, Cellular Stress, and Repression of Photosynthesis**

To understand the molecular implications and overall impact of the *friendly* mutation and of compromised fusion control on whole-cell homeostasis, we performed a set of microarray-based transcriptome studies on whole seedlings. Although, in general, only small fold changes of abundance in *friendly* relative to the wild type were observed, these changes were determined to be significant using Cybr-T (Baldi and Long, 2001) for 4,121 nonredundant transcripts (Supplemental Table S1). The significantly regulated transcripts were allocated to functional groups using MapMan (Usadel et al., 2005), resulting in the identification of 54 significantly regulated functional groups of genes (Table I). The functional groups included Protein Synthesis and Protein Degradation, consistent with the observed induction of autophagy. Together with Photosynthesis and Photosynthetic Light Reactions, which were also significantly regulated, this functional group set was identified previously by meta-analysis of multiple transcriptomic data sets (Schwarzländer et al., 2012a) as being a general indicator for mitochondrial dysfunction. In addition to these classes, we also observed regulation of Abiotic Stress, Redox, and Tricarboxylic Acid Cycle (Table I) that can be clearly linked to mitochondrial dysfunction. Interestingly, significant regulation was also determined for Transcription, including by the NAC (for NO APICAL MERISTEM/ARABIDOPSIS TRANSCRIPTION ACTIVATION FACTOR/CUP-SHAPED COTYLEDON) domain superfamily of transcription factors, members of which have been implicated in mitochondrial retrograde signaling (Tran et al., 2004; Chen et al., 2008; Nakashima et al., 2012; De Clercq et al., 2013; Ng et al., 2013).

The Activity of the Alternative Oxidase Pathway Is Increased in *friendly*

To determine the impact of the *friendly* mutation on mitochondrial respiration, and specifically on the alternative pathway, we measured oxygen uptake by whole seedlings in the aqueous phase using a Clark-type oxygen electrode. There was no significant difference in average oxygen uptake between the wild type ($25.5 \pm 3 \mu\text{mol oxygen h}^{-1} \mu\text{g}^{-1}$ chlorophyll) and *friendly* ($29.9 \pm 2.8 \mu\text{mol oxygen h}^{-1} \mu\text{g}^{-1}$ chlorophyll) under noninhibited baseline conditions (Fig. 9A). However, in the presence of 0.5 mM KCN, an inhibitor of the cytochrome pathway, average oxygen uptake by wild-type seedlings was reduced to $12.5 \pm 3.4 \mu\text{mol oxygen h}^{-1} \mu\text{g}^{-1}$ chlorophyll (Fig. 9A), a percentage inhibition of $51.2\% \pm 10.8\%$ (Fig. 9B), while average oxygen

uptake by *friendly* seedlings was only reduced to $25.3 \pm 4.3 \mu\text{mol oxygen h}^{-1} \mu\text{g}^{-1}$ chlorophyll (Fig. 9A), which was not a statistically significant change relative to uptake in the absence of KCN and equated to an inhibition of only $16\% \pm 8.5\%$ (Fig. 9B). This suggested that much of the oxygen uptake of *friendly* seedlings was due to the alternative pathway. To test this, we next measured the effect of 0.1 mM propylgallate, an inhibitor of the alternative oxidase, on the KCN-insensitive oxygen uptake. Propylgallate in combination with KCN reduced oxygen uptake by wild-type and *friendly* seedlings to approximately the same rate (3.4 ± 1.4 and $4 \pm 1 \mu\text{mol oxygen h}^{-1} \mu\text{g}^{-1}$ chlorophyll, respectively; $P = 0.498$), equating to a combined inhibition of KCN and propylgallate of baseline uninhibited oxygen uptake of approximately 87%, confirming that alternative oxidase induction is responsible for the KCN-insensitive oxygen consumption in *friendly* (Fig. 9B).

Photosynthetic Performance Is Reduced in *friendly* Due to a Defect in the External Electron Flow to PSI

To test the result from the transcriptome analysis suggesting photosynthetic defects in *friendly*, we next investigated PSI and PSII activities. There was no difference in steady-state PSII redox state between the wild type and *friendly*, as estimated by the chlorophyll fluorescence parameter $1 - q_L$ (fraction of open PSII centers [see "Materials and Methods"]; Fig. 9C). This observation was true both at the growth irradiance of $100 \mu\text{mol photons m}^{-2} \text{s}^{-1}$ and when the leaf being sampled was exposed to an actinic light of $910 \mu\text{mol photons m}^{-2} \text{s}^{-1}$ (Fig. 9C). Similarly, there was no difference in the capacity for nonphotochemical dissipation of excess light (nonphotochemical quenching) between the *friendly* mutant and the wild type (Fig. 9D).

PSI activity measured as the change in A_{820} was used to probe possible effects of the *friendly* mutation on PSI function and its supply of electrons. The wild-type plants exhibited a greater level of PSI activity (Table II) and an increased $\Delta A_{820}/A_{820}$ value. PSI was also more slowly reduced in *friendly*: this measure of how rapidly PSI is rereduced following the removal of far-red illumination indicates that PSI is receiving a diminished supply of electrons from plastocyanin and the photosynthetic electron transport chain. To probe whether the number of electrons available to PSI from the electron transport chain was diminished in *friendly*, we used the areas under the curve of the single- and multiple-turnover flashes. The results confirm the PSI rereduction observations, with *friendly* having a lower number of electrons available from sources outside of the linear electron transport chain (Table II).

FRIENDLY Is Lys Acetylated at Two Sites in the C-Terminal Region, Which Alters the Ability of FRIENDLY to Mediate Mitochondrial Association

A Lys-acetylated peptide of the FRIENDLY protein containing the two acetylation sites, Lys-1022 and

Table 1. Overview of significantly affected functional class gene bins

Mean log₂ fold ratios of transcripts were analyzed by functional class scoring for each experiment using MapMan software and applying the Hochberg correction. Numbers of transcript elements within each bin are indicated along with the *P* value.

Bin	Name	Elements	<i>P</i>
1	PS	142	6.87E-06
1.1	PS.lightreaction	90	1.81E-08
1.1.1	PS.lightreaction.photosystem II	41	1.72E-06
1.1.1.1	PS.lightreaction.photosystem II.LHC-II	13	1.71E-06
1.1.2	PS.lightreaction.photosystem I	16	0.005193416
1.1.2.2	PS.lightreaction.photosystem I.PSI polypeptide subunits	9	0.00185704
1.1.4	PS.lightreaction.ATP synthase	6	0.049475844
2.2.2	Major CHO metabolism.degradation.starch	25	0.002786643
8.1.1.1	TCA/org.transformation.TCA.pyruvate DH.E1	5	0.040470913
8.1.1.3	TCA/org.transformation.TCA.pyruvate DH.E3	4	0.016589986
10	Cell wall	484	2.07E-04
11.1.15	Lipid metabolism.FA synthesis	6	0.004793971
13.1.5.1.1	Amino acid metabolism	3	0.001269115
	Synthesis.Ser-Gly-Cys		
13.2.3.5	Amino acid metabolism.degradation	4	0.011276955
	Asp family.Lys		
13.2.4.4	Amino acid metabolism.degradation	4	0.010254625
	Branched-chain group.Leu		
16.8.4	Secondary metabolism.flavonoids.flavonols	18	0.033109368
17.7.3	Hormone metabolism.jasmonate.induced-regulated-responsive-activated	13	0.034124196
19.7	Tetrapyrrole synthesis.uroporphyrinogen decarboxylase	2	0.022203327
20.2.99	Stress.abiotic.unspecified	107	0.001724455
21.4	Redox.glutaredoxins	39	0.044251309
23.3.3	Nucleotide metabolism.salvage.NUDIX hydrolases	24	0.009327712
24.2	Biodegradation of xenobiotics.lactoylglutathione lyase	10	0.04597381
26.12	Misc.peroxidases	68	0.002081544
26.4	Misc.beta 1,3 glucan hydrolases	62	0.005670066
26.9	Misc.glutathione S transferases	50	0.013239802
27	RNA	2725	8.86E-06
27.3	RNA.regulation of transcription	2189	8.36E-04
27.3.3	RNA.regulation of transcription.AP2/ERE BP, APETALA2	112	0.010254625
27.3.27	RNA.regulation of transcription.NAC domain transcription factor family	18	0.032128735
29.2	Protein.synthesis	528	2.38E-14
29.5.11.20	Protein.degradation.ubiquitin.proteasome	60	8.26E-05
29.5.2	Protein.degradation.autophagy	23	0.002491643
30.2.3	Signaling.receptor kinases.Leu rich repeat III	41	0.022539336

Lys-1029, was identified in the analysis performed by Finkemeier et al. (2011; Supplemental Fig. S5). To validate the biological meaning of both sites and rule out artifacts, we studied the effect of Lys acetylation of Lys-1022 and Lys-1029 on the function of FRIENDLY by site-directed mutagenesis. The respective Lys residues were mutated to either Arg (to abolish Lys acetylation) or Gln (to mimic Lys acetylation), and the mutagenized cDNA coding sequences as well as the wild-type coding sequences were used to stably transform either *friendly* or its wild type followed by an analysis of mitochondrial clustering relative to overexpression or complementation (Fig. 10). The fact that the mitochondrial phenotype of wild-type plants is altered by overexpression of FRIENDLY suggests that FRIENDLY function is dependent on its expression level (Fig. 10B). Both K1022R and K1029R mutants were able to complement *friendly* to levels (44% and 38% for K1022R and K1029R, respectively) similar to the expression of the wild-type coding sequence (46%; Fig. 10). In contrast, mutation of either Lys

to Gln decreased complementation (29% and 6% for K1022Q and K1029Q, respectively) relative to the Lys-to-Arg mutants (Fig. 10A) or the wild-type coding sequence (Fig. 10B). The reverse results were obtained when wild-type plants were transformed with the site-directed mutants, indicating that only the Lys-to-Gln mutations can counter the clustered phenotype caused by overexpression in wild-type plants or transformation of the wild type with either Lys-to-Arg mutants (Fig. 10A) or the wild-type construct (Fig. 10B). The low level of complementation by the Lys-to-Gln mutants and the relative lack of effect of transformation with either of the Lys-to-Gln mutants in the wild type support the hypothesis that FRIENDLY activity can be regulated by Lys acetylation.

DISCUSSION

Regulation of mitochondrial movement and position within the cytosol has been demonstrated to be

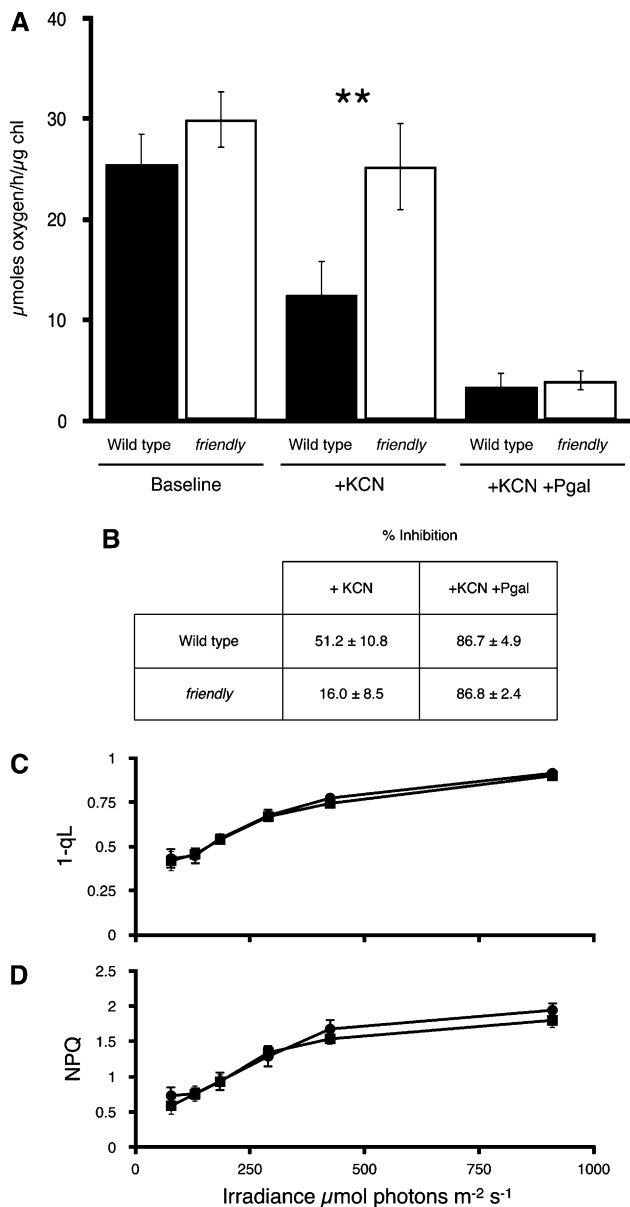


Figure 9. The activity of the alternative oxidase pathway is increased in *friendly*, but the activity of PSII is unaffected. A, Oxygen uptake in the wild type versus the *friendly* mutant under baseline conditions or in the presence of 0.5 mM KCN or 0.5 mM KCN plus 0.1 mM propylgallate (Pgal). The rate of oxygen uptake in the presence of KCN was significantly different between the wild type and *friendly* (** $P < 0.01$). Error bars indicate sd ($n = 4$). chl, Chlorophyll. B, Percentage inhibition of respiration in the wild type and *friendly* relative to the baselines values, calculated using the data depicted in A. C, Steady-state PSII redox state (as estimated by the chlorophyll fluorescence parameter $1 - q_L$) in the wild type and *friendly*. D, Capacity for nonphotochemical dissipation of excess light (NPQ) in *friendly* and the wild type.

essential for correct mitochondrial and cellular function (Boldogh and Pon, 2007; Frederick and Shaw, 2007; Logan, 2010b; Shutt and McBride, 2013). Moreover, mitochondria display altered motility and distribution

under stress conditions, or when their function is impaired, in a variety of cell types across diverse eukaryote lineages (Chen and Chan, 2009; Nunnari and Suomalainen, 2012). For example, in *Arabidopsis*, clustering and arrest of mitochondrial movement has been identified as a response to biotic and abiotic stress: in response to UV light exposure (Gao et al., 2008), to the presence of methyl jasmonate (Zhang and Xing, 2008), following treatment with the oxylipin, 9-hydroxy-10,12,15-octadecatrienoic acid (Vellosillo et al., 2013), and in response to heat shock or the application of reactive oxygen species (Scott and Logan, 2008). Mitochondrial dynamics, therefore, is not only key to cell function but also to the cellular response to stress. Here, we provide new insights into the effects of mitochondrial clustering induced by mutation of the *Arabidopsis* CLU-type *FRIENDLY* gene and evidence for the role of this gene in regulating mitochondrial association and fusion.

Work on *Dictyostelium discoideum* first identified the involvement of *FRIENDLY*-like (CLU-type) genes in the maintenance of mitochondrial distribution (Zhu et al., 1997). As a result of TEM analysis of clusters in the *D. discoideum* *cluA*⁻ mutant showing continuity of the outer mitochondrial membrane of adjacent mitochondria, and sometimes penetration of the inner membrane between such connected mitochondria, it was concluded that CluA was involved in mitochondrial division (Fields et al., 2002). While we sometimes see an electron-dense patch between adjacent mitochondria by TEM of leaf tissue fixed by high-pressure freezing, we do not see any obvious outer membrane connectivity between mitochondria in high-pressure freezing-fixed material (this work), nor did we with chemically fixed leaves (Logan et al., 2003). In addition, the lack of mito-GFP fluorescence recovery in our photobleaching experiments confirms a lack of matrix continuity between adjacent mitochondria in a cluster. Fields et al. (2002) cited the similarity of the mitochondrial organization in yeast *clu1Δ* cells to that in cells lacking the mitochondrial division protein Dynamin1 as further evidence of a role for CluA in mitochondrial division in *D. discoideum*. However, applying the same argument to *Arabidopsis* leads to the opposite conclusion. *Arabidopsis* mutants of proteins involved in mitochondrial division, such as the dynamin-like proteins Dynamin Related Protein 3A (DRP3A; Logan et al., 2004) and DRP3B (Arimura and Tsutsumi, 2002), the FISSION1 ortholog BIGYIN1 (Scott et al., 2006), or the plant-specific protein NETWORK MITOCHONDRIA1 (Logan et al., 2003; Arimura et al., 2008), contain greatly enlarged, elongated, or reticular mitochondria, completely different from the clustered mitochondrial phenotype of *friendly* mutants. Notwithstanding the lack of evidence for a membranous connection between mitochondria in a cluster, the fact that clusters can move through the cytosol as units demonstrates that individual mitochondria in a cluster are physically associated, as suggested by our observation of electron-dense patches between mitochondria visualized by TEM. While the specific identities of the proteins involved in this

Table II. *PSI activity is reduced in friendly*

Values shown are means \pm SE ($n = 10$ independent biological replicates). For experimental details, see "Materials and Methods."

Plant Line	$\Delta A_{820}/A_{820}$ ^a	Half-Time of PSI Rereduction ^b	Intersystem e ⁻ Pool e ⁻ /P700
	<i>relative units</i>	<i>ms</i>	MT_{area}/ST_{area}
Wild type	570 \pm 17	73 \pm 4	20.9 \pm 2.5
<i>friendly</i>	509 \pm 25	86 \pm 6.7	15.1 \pm 1.3

^aThe $\Delta A_{820}/A_{820}$ ratios are significantly different ($P = 0.03$). ^bThe half-time values are significantly different ($P = 0.04$).

physical intermitochondrial association, which we term a "handshake," are currently unknown, it is clear that FRIENDLY is required to regulate handshake duration and, therefore, the speed that mitochondria can undergo complete kiss-and-run fusion and division events that shape the plant chondriome. In *friendly*, all mitochondria appear to have an increased tendency to stick to another, relative to the wild type, causing an increase in the association time between any two mitochondria and thereby accounting for similar pulsing rates of discrete and clustered mitochondria and resulting in cluster formation (as confirmed by modeling). Future experiments will seek to identify proteins interacting with FRIENDLY that may be involved in the intermitochondrial stickiness that causes them to aggregate if movement on the actin cytoskeleton is disrupted (e.g. by actin depolymerization). These same proteins also may be involved in the change of mitochondrial distribution and motility that results from biotic and abiotic stress. Our discovery that FRIENDLY can be Lys acetylated and that preventing acetylation by mutation of either of the two acetylation sites to Gln significantly decreases (and Arg increases) the molecular complementation, relative to the effect of expressing the wild-type coding sequence, suggests that one mechanism to regulate intermitochondrial stickiness may be changing the acetylation state of FRIENDLY.

No components of the plant mitochondrial fusion apparatus have been identified, despite genetic and cell biological evidence that fusion occurs in plants. For example, fusion enables mitochondrial DNA (mtDNA) transfer between physically discrete organelles, and this transfer supports the high degree of recombination activity in mitochondrial genomes (Lonsdale et al., 1988). That such fusion-driven recombination takes place in plants has been shown by the identification of novel nonparental arrangements of mtDNA in cybrids resulting from protoplast fusion (Belliard et al., 1979; Aviv and Galun, 1987). Indeed, it has recently been argued that the massively expanded mitochondrial genomes of higher plants such as *Amborella trichopoda*, which contains the entire mitochondrial genomes of other plant species (Rice et al., 2013), is a result of mtDNA recombination facilitated by mitochondrial fusion. In addition to the size and complexity of plant mitochondrial genomes relative to nonplant eukaryotes, it has been shown that mtDNA is unevenly distributed among the population of several hundred physically discrete organelles, with some mitochondria containing

less than a full genome (Lonsdale et al., 1988; Arimura et al., 2004). This heterogeneity led to the plant chondriome being termed a dynamic syncytium (Lonsdale et al., 1988) or a discontinuous whole (Logan, 2006) to describe the functional interdependence of the physically discrete organelles. This interdependence has been suggested to drive a need to meet, such that there is a requirement for mitochondria to be mobile so that they can associate with and then fuse with one another to enable the transfer of mtDNA (Logan, 2010b).

The ability of mitochondria in the *friendly* mutant to meet in order to fuse is disrupted by at least three mechanisms: first, the size of the clusters hampers their movement through the densely packed cytosol; second, many mitochondria within the inner reaches of a cluster can only associate with their equally trapped neighbors

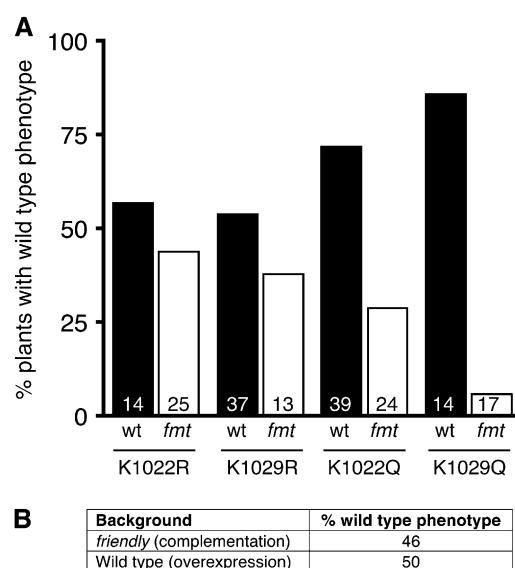


Figure 10. Lys acetylation alters the ability of FRIENDLY to mediate mitochondrial association. A, Quantification of the percentage of wild-type (wt) and *friendly* (*friendly mitochondria* [*fmt*]) plants displaying a wild-type phenotype when stably transformed with transgenes encoding for mutant FRIENDLY proteins incorporating a Lys-to-Gln or Lys-to-Arg mutation at residue 1,022 or 1,029. Numbers within each bar are the numbers of T1 individuals identified within each transgene/background combination. B, Percentage of T1 plants (22 individuals were analyzed) displaying a wild-type phenotype after transformation with 35S-FRIENDLY of either *friendly* (complementation) or the wild type (overexpression).

until clusters are broken apart by shear forces of F-actin remodeling or by transport through physical bottlenecks in the cytosol; third, the increased association/handshake time in *friendly* necessarily decreases the number of new associations and thus new, rather than repeated, fusion events that can take place in a given time period. Our analysis of fusion shows that there is a significant increase in the exchange of matrix-localized photoconverted mEos (and thus a greater reduction in the average number of green mitochondria) in the *friendly* chondriome relative to the wild type. Our interpretation of these data is that although mitochondria in different regions of the cell are less likely to meet in *friendly*, when they do meet they stay associated for longer (increased handshake duration), forming clusters of potential fusing partners, which increases the number of fusion events even though these events are unlikely to generate as even a mixing of mitochondrial matrix within the chondriome as occurs in the wild type. In addition to the fusion assay and handshake data, the results of our analysis of mitochondrial membrane potential pulsing suggest that mitochondrial fusion is disrupted in *friendly*. Santo-Domingo et al. (2013) presented evidence that transient depolarization and matrix alkalization (pulsing) represented the formation of a fusion initiation pore within the mitochondrial inner membranes, which is not necessarily followed by an exchange of matrix constituents. The absence of the pro-fusion protein Optic Atrophy1; Alexander et al., 2000; Delettre et al., 2000) completely abolished pulsing (Santo-Domingo et al., 2013). Therefore, the 100-fold increase in pulsing rate in *friendly* may be indicative of either actively stimulated fusion initiation or loss of control over that process. That putative fusion pore opening is so much more frequent in *friendly* may be due to the increased duration that fusion-defective mitochondria are associated (handshake) with one another. Given the absence in plants of homologs of pro-fusion factors present in other eukaryotes (including OPA1), *friendly* is thus a powerful genetic tool with which to dissect the precise physiological role of pulsing and the role of FRIENDLY in plant mitochondrial fusion in general.

friendly displays numerous indicators of stress, such as an increased number of dead root cells, increased number and size of acidic compartments, tentatively identified as autolysosomes, and the increased frequency of mitochondrial membrane potential pulses. Further evidence for *friendly* being affected by stress is displayed on the transcriptomic level, including significant regulation of functional gene groups previously identified as targets of mitochondrial dysfunction and oxidative stress (Schwarzländer et al., 2012a). Lack of the *D. melanogaster* FRIENDLY ortholog in the *clu* mutant also leads to mitochondrial oxidative stress as measured by strongly decreased aconitase activity (Sen et al., 2013).

A recent study provides additional evidence regarding the importance of chondriome dynamics, and FRIENDLY in particular, this time in the response to biotic stress. A mutant allele of FRIENDLY (*noxy38*)

was identified in a screen for insensitivity to the oxylipin pathogen defense mediator 9-hydroxy-10,12,15-octadecatrienoic acid in Arabidopsis (Vicente et al., 2001; Vellosillo et al., 2013). The *noxy38* mutant showed an up-regulation of alternative oxidase expression and a decreased capacity to fight bacterial infection (Vellosillo et al., 2013). Interestingly, a mutant of the mitochondrial division protein DRP3A, with a chondriome comprising elongated and interconnected mitochondrial tubules, was identified in the same screen, suggesting that chondriome structure per se is important for plant defense responses to pathogens. Taken together, the disruption of mitochondrial chondriome structure in response to biotic and abiotic stress (Gao et al., 2008; Scott and Logan, 2008; Zhang and Xing, 2008), the reduced ability of plants with altered chondriome structure to fight pathogen attack (Vellosillo et al., 2013), and the stress phenotypes in the *friendly* mutant (this work) suggest that in plants, as in animals (Runkel et al., 2013; Liu et al., 2014), mitochondria perform the role of sentinels whereby disruption of mitochondrial function is interpreted as an attack on the cell and that chondriome structure is important for the defense response.

CONCLUSION

We show here that the clustered mitochondrial phenotype in the *friendly* mutant arises by increased duration of intermitochondrial handshake events. We propose that FRIENDLY is an important component of the mitochondrial kiss-and-run fusion apparatus and functions by regulating intermitochondrial association. No other gene involved in mediating the fusion of plant mitochondria is currently known. Furthermore, we provide preliminary evidence that FRIENDLY function may be regulated by Lys acetylation, thereby controlling the association of FRIENDLY with mitochondria. Future experimentation refining the role of FRIENDLY Lys acetylation may thus lead to a greater mechanistic understanding of the dynamic regulation of chondriome structure and its effects on cell physiology. In summary, we have provided several independent lines of strong evidence that FRIENDLY functions in mitochondrial homeostasis by maintaining normal mitochondrial distribution, motility, and fusion via the regulation of intermitochondrial association time.

MATERIALS AND METHODS

Plant Materials and Growth Conditions

All experiments using Arabidopsis (*Arabidopsis thaliana*) were conducted using the Columbia-0 (Col-0) ecotype. Except when used for transformation, Arabidopsis seeds were first germinated on agar under aseptic conditions as follows. Seeds were surface sterilized by washing in 80% (v/v) ethanol for 5 min with continual inversion, and this wash was replaced with 30% (v/v) household bleach before three rinses in sterile type III water. Seeds were spread on plates and stratified as described by Logan et al. (2003) before moving to a growth chamber at 23°C under a 16-h-light/8-h-dark photoperiod using cool-white light at 100 $\mu\text{mol m}^{-2} \text{s}^{-1}$. For transformation, Arabidopsis seeds were stratified before direct sowing on a 1:1 compost (Sunshine LG3;

www.sungro.com):vermiculite mixture. Plants to be crossed were first grown on agar as above before transplanting after 2 weeks to the compost:vermiculite mixture. Tobacco (*Nicotiana tabacum*) seeds were also sown directly on this compost:vermiculite mixture and transferred to a growth chamber at 23°C under a 16-h-light/8-h-dark photoperiod using cool-white light at 150 $\mu\text{mol m}^{-2} \text{s}^{-1}$.

friendly Ethyl Methanesulfonate and T-DNA Insertion Lines

friendly was identified in a microscope-based screen of a mito-GFP line mutated with ethyl methanesulfonate (Logan and Leaver, 2000; Logan et al., 2003). The mutant allele was identified by map-based cloning and DNA sequencing as At3g52140 bearing a single G-to-A mutation in the first intron-exon boundary (Logan et al., 2003). The *friendly* mutant was backcrossed to its wild type (mito-GFP), and the homozygous recessive mutant was reidentified five times to clean up the genetic background (Feldmann et al., 1994). T-DNA Express (<http://signal.salk.edu/cgi-bin/tdnaexpress>) was used to identify the T-DNA insertion line SALK_046271 bearing an insertion in the 18th intron of the *FRIENDLY* gene (At3g52140), and seed was obtained from the Arabidopsis Biological Resource Center (<http://www.arabidopsis.org/>). Homozygous mutant plants (named *friendly-3*) were identified using the gene-specific LP (5'-ATACCTGCAGCAGTTTGAAC-3') and RP (5'-CTAGCGCCAACAGCTCTACTG-3') primers together with the left border T-DNA primer (LBb1), 5'-GCGTGGACCGCTTGCTGCAACT-3'. Homozygous *friendly-3* mutants were crossed with lines expressing mito-GFP or mito-mEosFP (using the same targeting signal as mito-GFP but fused to mEos; Mathur et al., 2010). Crossing was performed as described by Meyerowitz and Somerville (1994).

FRIENDLY Cloning

Total RNA was extracted from 14-d-old Arabidopsis Col-0 seedlings using the RNeasy Plant Mini Kit (Qiagen). RNA was reverse transcribed using ThermoScript reverse transcriptase according to the manufacturer's instructions (Life Technologies).

FRIENDLY was amplified from cDNA using Phusion DNA polymerase (New England Biolabs) and the following primers: forward, 5'-ATGCTGGGAAGTCGAACAAATCGAAGGCCAAG-3', and reverse 5'-TTATTTTTGGCTTTTGTCTTCTTATCCAAG-3'. A PCR product of the expected size was amplified, gel purified, and cloned using the Zero Blunt Topo PCR Cloning Kit (Life Technologies). Putative positive clones were cultured overnight before plasmid extraction and restriction digest analysis using *Hind*III. DNA sequencing followed to identify an error-free clone, named pCR-FRIENDLY, which was 100% identical to the coding sequence of gene model At3g52140.1 in the database of The Arabidopsis Information Resource (<http://www.arabidopsis.org/servlets/TairObject?id=37255&type=locus>).

Amplification of FRIENDLY cDNA for Gateway Fluorescent Fusion Constructs and Site-Directed Mutagenesis

pCR-FRIENDLY was used as the template for recloning with Gateway attB primers. The PCR product was gel purified, recombined into pDONRzeocin (Life Technologies) to give pDONRz-FRIENDLY, and transformed into *Escherichia coli*. Positive clones were identified as above and subjected to DNA sequencing to confirm error-free amplification. pDONRz-FRIENDLY was recombined with the Gateway destination binary vectors pMDC83, pDCLmrfp1-X, and pDCLX-mrfp1 (modified versions of pMDC43 and pMDC83, respectively [Curtis and Grossniklaus, 2003]; http://botserv1.uzh.ch/home/grossnik/curtisvector/index_2.html), to generate a C-terminal translational fusion to modified (m)GFP6 and N- and C-terminal fusions to mRFP1, and with pMDC32 for FRIENDLY overexpression and complementation experiments. Positive clones were identified and verified as described above.

Site-Directed Mutagenesis

Site-directed mutagenesis of *FRIENDLY* (in pDONRz-FRIENDLY) to convert Lys-1022 or Lys-1029 to Gln or Arg was performed using the GeneTailor Site-Directed Mutagenesis Kit (Life Technologies) following the manufacturer's instructions and using the oligonucleotide primers listed in Supplemental Table S1. The mutated cDNAs were cloned using Gateway technology (Life Technologies) into pMDC32, which was used to stably

transform *friendly* and its wild type (mito-GFP line 43C5, expressing a translational fusion of 93 N-terminal amino acids of the β -ATPase subunit of *Nicotiana plumbaginifolia* to mGFP5; Logan and Leaver, 2000) as described below.

Live Cell Imaging

Live imaging (except FRAP, pulsing analysis, and the in vivo fusion assay) used one of two microscope systems. System 1 consisted of an Olympus BX61 with a 100 \times U-PLAN S-APO oil-immersion objective (numerical aperture [NA] = 1.4), Semrock Brightline cubes for GFP (excitation, 473/31 nm; dichroic, 495 nm; emission, 520/35 nm) and mRFP/mCherry (excitation, 543/22 nm; dichroic, 563 nm; emission, 593/40 nm) and X-Cite exacte illumination. Images were captured with a QImaging Rolera-MGi Plus EMCCD camera attached to a computer work station running Metamorph.

System 2 consisted of a Zeiss META 510 confocal laser-scanning microscope (Carl Zeiss, MicroImaging) driven by a personal computer running LSM510/ConfoCor2 software, version 3.2. The microscope was equipped with 25 \times and 63 \times water-immersion objectives (NA = 1.2). GFP was excited with the 488-nm argon laser (HFT 405/488/543 dichroic), and emission was collected between 505 and 530 nm. PI-stained tissue was excited using the 488-nm argon laser (HFT 405/488/543 dichroic), and emission was collected between 610 and 660 nm. LysoTracker-stained tissue was excited using the 543-nm helium-neon laser (HFT 405/488/543 dichroic), and emission was collected between 585 and 650 nm. SYTOX Orange-stained tissue was excited with the 514-nm laser (488/514 dichroic), and emission was collected between 560 and 615 nm.

IMARIS 7.4.2 software (Bitplane) was used for image analysis and three-dimensional reconstructions. Images were deconvolved using AutoQuant X2 (MediaCybernetics) as appropriate.

Transformation of Arabidopsis

Binary vectors were used to transform electrocompetent *Agrobacterium tumefaciens* (strain GV3101), and positive clones were identified by restriction digestion as above following a modified plasmid extraction protocol. Wild-type (Col-0), mito-GFP (Logan and Leaver, 2000), or *friendly* ethyl methanesulfonate mutant (which is in the mito-GFP background; Logan et al., 2003) plants were transformed using the floral dip method (Clough and Bent, 1998). Transformed plants were selected on appropriate antibiotics and then screened by fluorescence microscopy, if appropriate, using microscopy system 1.

Transient Transformation of Tobacco Leaf Cells

Fluorescent protein fusion constructs were transformed into tobacco (*Nicotiana tabacum*) leaves using agroinfiltration with a variety of *A. tumefaciens* cell densities and the method described by Sparkes et al. (2006). Microscopy using system 1 was performed 3 to 4 d after infiltration. Peroxisomes were visualized using the construct pRCS2/mCherry-PTS1 (a kind gift from Dr. Robert Mullen, University of Guelph), ER using er-RB (an mCherry-HDEL construct; Arabidopsis Biological Resource Center stock no. CD3-960; Nelson et al., 2007), and Golgi using ST-mRFP1 (Teh and Moore, 2007).

Transient Transformation of Arabidopsis Seedlings

Seedlings of *friendly* were transformed essentially as described by Candat et al. (2014), except that 0.01% (v/v) Silwet L-77 was used instead of Tween 20. Microscopy of transformed seedlings was performed using a Nikon A1 confocal laser-scanning microscope equipped with a 40 \times water-immersion objective (NA = 0.9) and using 488- and 561-nm excitation for GFP and mRFP1, respectively.

TEM

Sections of the true leaves of 14-d-old Arabidopsis seedlings were high-pressure frozen at the Biotechnology and Biological Sciences Research Council Oxford Brookes High Pressure Freezing Facility using a Baltec HPPF10 apparatus and freeze substituted in the presence of 2% (w/v) osmium using an AFS apparatus (Leica) as described by Tse et al. (2006). After freeze substitution, sections were embedded, sectioned, and observed by TEM according to Osterrieder et al. (2010).

Cluster Size and Number in the Wild Type and *friendly*

Epidermal cells of 7-d-old *friendly* plants and their wild type were imaged using microscopy system 1. Images were obtained from 40 randomly chosen independent seedlings of each line. Mitochondrial clusters or groups were quantified using the Analyze Particles command in Fiji (ImageJ) software (Schindelin et al., 2012). Clusters of mitochondria in *friendly* were minimally defined as discrete particles consisting of mitochondria covering an area of at least $2.5 \mu\text{m}^2$. Groups of wild-type mitochondrial were defined as discrete particles covering an area of at least $0.2 \mu\text{m}^2$.

FRAP

For FRAP, we used a Zeiss LSM 410 inverted confocal laser-scanning microscope (Carl Zeiss, MicroImaging) equipped with 25 \times and 63 \times water-immersion objectives (NA = 1.2) and driven by a personal computer running LSM410/Zeiss LSM software. GFP was excited with the 488-nm argon laser (HFT 488/594 dichroic), and emission was collected between 505 and 530 nm. Leaf epidermal pavement cells of 7-d-old seedlings were used. A portion of a randomly chosen mitochondrial cluster of *friendly*, or of a tubule in the *network* mutant, was bleached using 80% argon laser power followed immediately by a reduction of the argon laser power to 10% and capture of 300 images 1 s apart to observe any GFP recovery.

Cytoskeleton and Mitochondria Visualization

In order to visualize actin filaments and mitochondria, a double transgenic line was generated by crossing mito-GFP with a second line (mCherry-mTn) expressing an in-frame fusion of mCherry (Shaner et al., 2004) to the C-terminal 197 amino acids of mouse talin, which forms the actin-binding domain. The mCherry-mTn line was generated by transformation of Arabidopsis Col-0 with pDCLmcherry-mTn. The backbone of pDCLmcherry-mTn, the pDCLmcherry-X destination vector, was a modified pMDC43 (Curtis and Grossniklaus, 2003) in which mGFP6 was replaced by mCherry via pMDC7 and pMDC24. A cDNA fragment encoding the mTalin actin-binding domain was PCR amplified from the pZP202-GFP-mTn vector (Kost et al., 1998) using attB Gateway primers and recombined into pDONRz. Recombination between pDONRz-mTn and pDCLmCherry-X created pDCLmcherry-mTn. Actin and mitochondria were imaged using microscopy system 1.

To visualize microtubules, we PCR amplified, using Gateway attB primers, MICROTUBULE-ASSOCIATED PROTEIN4 (MAP4; Olson et al., 1995) from a GFP-MAP4 construct that was a kind gift from Jaideep Mathur (University of Toronto; Mathur and Chua, 2000). The MAP4 cDNA was recombined with pDONRz, which in turn was recombined with the pDCLmcherry-X destination vector. A stable Arabidopsis line expressing mCherry-MAP4 was crossed with mito-GFP or with the *friendly* mutant expressing GFP, and the crossed lines were analyzed using fluorescence microscopy. To visualize the plus end of microtubules, we PCR amplified, using attB1 primers, the End Binding Protein 1b (EB1b) coding sequence from GFP-EB1b (Mathur et al., 2003), and this was cloned and recombined with pDCLmcherry-X as above. A stable Arabidopsis line expressing mCherry-EB1b was crossed to the wild type and *friendly* as above.

Measurement of Mitochondrial Association Time

Movies were generated from 250 images of the control mito-GFP line or *friendly* captured at 1-s intervals using microscopy system 1. Five movies were captured of different regions of the epidermis of the true leaves of three 7-d-old seedlings to give 15 movies (technical replicates). The results presented are means of associations measured in three independent experimental repeats each composed of 15 movies ($n = 3$). Association time was calculated as the number of frames (seconds), counted from the time a single mitochondrion was within one mitochondrial width of either a second mitochondrion in the case of the wild-type mito-GFP line or of a mitochondrion at the exterior surface of a cluster of mitochondria in the case of *friendly*, until the same mitochondrion moved at least one mitochondrial width from its partner(s).

Dynamic Model of Plant Mitochondrial Dynamics

The dynamic model consists of a set of n model mitochondria positioned on an $1 \times 1 \times 1$ cubic lattice with periodic boundary conditions. Two or more

mitochondria cannot occupy the same lattice site. A mitochondrion is labeled as free if none of its six nearest neighbor sites are occupied by another mitochondria; otherwise, it is labeled as clustered. The model is initialized by placing the n mitochondria randomly on the lattice. We use the Gillespie stochastic simulation algorithm (Gillespie, 1977) to simulate the subsequent dynamics of the model, with each mitochondrion able to move to any of its empty nearest neighbor sites. The rate with which a free mitochondrion moves to a given neighbor is λ_1 , and the rate with which a clustered mitochondrion moves to a given neighbor is λ_2 . If mitochondria are very sticky, then λ_2/λ_1 will be much less than 1. The algorithm is run until the number of clustered mitochondria converges to a steady state, n_c . We also define the association time τ as the time interval between an initially free mitochondrion first becoming clustered and thereafter becoming free. We record the average association time over all mitochondria and over simulation time. We use $l = 20$, $n = 400$, and $\lambda_1 = 1$ for these simulations; the results are qualitatively robust across the full range of other reasonable parameterizations (data not shown). We vary λ_2 , running 20 Gillespie simulations for each value, and record mean values of cluster proportion $c = n_c/n$ and τ .

Pulsing Measurement and Analysis

Seedlings were grown on vertical plates containing 0.5 \times Murashige and Skoog (MS) medium + 0.8% (w/v) phytigel. The membrane potential of mitochondria in living tissue was determined by CSLM using the red fluorescent potentiometric dye TMRM that accumulates reversibly in mitochondria in response to the inner membrane potential (Brand and Nicholls, 2011). After 4 d, seedlings were incubated in freshly prepared 50 nM TMRM for more than 15 min before confocal imaging of roots bathed in fresh probe. Confocal microscopy, performed using a Zeiss LSM 780 confocal microscope (Carl Zeiss, MicroImaging), and data analysis were performed as described previously (Schwarzländer et al., 2012b).

In Vivo Mitochondrial Fusion Assay

Exchange of matrix-localized mito-mEosFP (Mathur et al., 2010) was analyzed between mitochondria in the leaves of 14-d-old Arabidopsis seedlings. Pieces of detached leaf were mounted in water between a slide and a coverslip on a chambered slide made from two parallel strips of ultrathin double-sided adhesive tape (Ekanayake et al., 2014). Imaging was performed using a Nikon A1 confocal laser-scanning microscope fitted with a 40 \times (NA = 1.25) water-immersion objective and using the photoconversion dialogue within the Elements software package. Two frames ($1,024 \times 1,024$ pixels) were captured preconversion at 0.25 fps (pixel dwell time of 2.4 μs). Photoconversion was performed at 0.25 fps (pixel dwell time of 2.2 μs) within a rectangular region of interest using the 405-nm laser at 40% power output and for a total of 6 s. After photoconversion, image capture continued for 72 loops equating to 4.39 min. Green and red channels were captured simultaneously preconversion and postconversion using a 488-nm laser at 1% and a 561-nm laser at 1.5%, respectively. CSLM time courses were saved as .avi files and analyzed using a custom-designed Matlab program (Schwarzländer et al., 2012b). Green-red ratios were calculated for an identical number of pixels covered by each identified mitochondrion in each of the 74 movie frames of each biological replicate. The green-red pixel ratio was calculated for each identified mitochondrion at each time point. Calculation of the numbers of green mitochondria used a threshold of average + SD of the green-red pixel ratio preconversion. The initial and final percentages of green mitochondria postconversion were calculated using the average of the first three (i.e. frames 4, 5, and 6) or the last three (i.e. frames 72, 73, and 74) time points, respectively.

Whole-Plant Phenotyping

To measure the rate of plant root growth, seeds were germinated and grown on aseptic agar plates as described above, with the plates maintained in a vertical orientation so that the roots grew along the surface of the agar. Measurements were made of 20 seedlings (technical replicate) for each time point per experiment (biological replicate), and the results presented are means of the three biological replicates. Wild-type mito-GFP or Col-0 were used as controls for *friendly* or *friendly-3*, respectively. To measure etiolated hypocotyl length, seeds were germinated and grown on MS agar plates in the dark (plates covered with aluminum foil). Hypocotyl length was measured after 7 d, and technical and biological replication was as described for root length. To measure biomass, seeds were germinated and grown on MS agar plates as above for 7, 14, 21, or 28 d. At each time point, free surface moisture of 15

seedlings was removed gently using a soft paper towel before their total fresh weight was recorded. The seedlings were then completely dried and reweighed. The experiment was repeated three times, and the results presented represent the mean ($n = 3$).

Root Cellular Structure and Cell Viability Measurements

Whole seedlings (6 d old) were stained in PI solution ($3 \mu\text{g mL}^{-1}$) for 2 min followed by a quick wash in distilled water. Stained roots were mounted in water between the slide and coverslip and observed by CSLM.

To visualize dead cells using SYTOX Orange, roots of 6-d-old seedlings were stained in 250 nM SYTOX Orange (Life Technologies) for 20 min followed with a quick washing step in distilled water. Z-stacks were captured by CSLM using imaging parameters as described above, and the number of dead cells, as visualized by a SYTOX Orange-stained nucleus, was counted in the root cap, division zone, elongation zone, and differentiating zone.

Staining of Acidic Compartments Using LysoTracker

Arabidopsis mito-GFP and *friendly* were grown on MS agar for 6 d. Seedlings were stained with $1 \mu\text{M}$ LysoTracker Red DND-99 (Life Technologies) in $0.5\times$ MS medium for 5 min at room temperature to visualize acidic compartments. After staining, the seedlings were washed with distilled water to remove excess stain. The root cells (elongation zone) were visualized by CSLM. LysoTracker-stained structures were analyzed using the Analyze Particles command in Fiji (ImageJ).

Arabidopsis Oligonucleotide Microarray

Seeds of Arabidopsis (*friendly* and mito-GFP) were germinated and grown as described above. Both lines were grown under the same conditions, and 0.1 g of leaves was harvested from each of four plates (each representing a biological replicate) and then frozen in liquid nitrogen immediately before RNA isolation using the RNeasy Plant Mini Kit according to the manufacturer's protocol. The RNA samples representing four biological replicates of each line (*friendly* and mito-GFP) were labeled (two cy3 and two cy5) and hybridized to slides prepared by the University of Arizona following the protocol described at <http://ag.arizona.edu/microarray>. Scanning, image analysis, and quantification were as described previously (Xiang et al., 2011). Raw data were saved as a .gpr file and converted into an .mef file using the Express Converter software (version 2.1; Dana Faber Cancer Institute). Data were normalized using the Lowess (locfit) algorithm and block normalization in the MIDAS software (version 2.22; Dana Faber Cancer Institute). Duplicates in the data set were removed by averaging intensity values using the FiRe macro (Garcion et al., 2006). Significantly regulated transcripts were detected using Cybr-T Bayesian probabilistic framework analysis (Baldi and Long, 2001; Bayes $P < 0.05$). Functional class scoring was implemented using MapMan software (Thimm et al., 2004) applying the Benjamini-Hochberg correction. The data sets were deposited at the European Bioinformatics Database ArrayExpress database according to the Minimum Information about a Microarray Experiment guidelines.

Respiration

Seeds of the wild type or *friendly* were germinated and grown hydroponically for 7 d as described by Benamar et al. (2013). Oxygen uptake was measured in the same growth medium using a Clark-type oxygen electrode (Hansatech). Cyanide-sensitive oxygen uptake was measured in the presence of 0.5 mM KCN before the addition of propylgallate to 0.1 mM. Total chlorophyll content ($\mu\text{g mL}^{-1} = 7.04 \times A_{664} + 20.27 \times A_{647}$) was measured using the dimethylformamide method of Moran (1982). Measurements were made using four biological replicates ($n = 4$), and data are presented as means \pm SD.

Analysis of Photosynthesis

Plants were grown as described above. Fully developed rosette leaves were placed in the dark for 15 min prior to determining dark-adapted initial and maximum PSII fluorescence (F_o and F_m). All measurements were performed using an XE-PAM system (Heinz Walz), and the data were collected via the PAM-Data Acquisition System (PDA-100) interfaced with the WinControl Software version 2.08 (following the manufacturer's instructions). To induce

minimal fluorescence, the weak modulated light source was turned on and data were collected for 30s. Once the signal had stabilized, an 800-ms pulse of $4,000 \mu\text{mol photons m}^{-2} \text{s}^{-1}$ was applied to the leaf to close the PSII reaction centers and generate F_m . The leaf was then exposed to an actinic light source until a steady-state level of fluorescence was reached (F_s). To estimate the fraction of closed PSII reaction centers at steady state, a saturating flash was applied and maximum PSII fluorescence in the light-adapted state (F_m') was determined. Following the saturating flash, the actinic light was removed and a weak far-red light (102-FR; Heinz Walz) was applied to oxidize the electron transport chain. When a steady state was reached, F_o' was determined. The actinic light intensity was then increased and the same steps were repeated. The dark-adapted optimal quantum yield of photosynthesis was calculated as variable PSII fluorescence in the dark-adapted state (F_v)/ F_m according to the equation $[F_v/F_m = (F_m - F_o)/F_m]$; van Kooten and Snel, 1990; Krause and Weis, 1991). The relative redox state of PSII at steady state was estimated at each light level using the term $1 - qL$, where $qL = (F_m - F_s)/(F_m - F_o) \times (F_o/F_s)$ (Kramer et al., 2004). Similarly, the amount of nonphotochemical quenching was estimated at each light level using the term NPQ, where $\text{NPQ} = (F_m - F_m')/F_m$ (Genty et al., 1990).

To estimate the functional activity of PSI in *friendly*, fully developed rosette leaves from the same plants used for PSII analyses were examined using a PAM-101 control unit equipped with the ED-P700DW Dual-Wavelength-P700 emitter/detector (Heinz Walz). Data were collected using the PDA-100 interfaced as described (Ivanov et al., 1998; Schreiber et al., 1988). Far-red light was applied to the leaf using the 102-FR light source. The deflection in the signal ($\Delta A_{820}/A_{820}$) was used to estimate the amount of oxidizable P700 (Schreiber et al., 1988). The functional pool size of intersystem electrons was determined by applying single-turnover (ST) and multiple-turnover (MT) flashes (Asada et al., 1992; Ivanov et al., 1998). The single-turnover flash had a one-half-peak width of 10 μs produced by the XE-Pump Flash Control Unit (XE-STC; Heinz Walz). The multiple-turnover flash had a duration of 50 ms. Both flashes were produced using the XMT-103 power/control unit (Heinz Walz). The number of intersystem electrons per P700 was calculated using the equation $e^-/\text{P700} = \text{MT}_{\text{area}}/\text{ST}_{\text{area}}$. The areas under the curve were calculated using the Origin 9.0 software package (OriginLab). The relative rate of P700 reduction following removal of the far-red light was calculated by finding the time required to reach one-half of the dark reduction level and thus is presented as a half-time value (Berry et al., 2011).

Lys Acetylation

Experimental details for the extraction of proteins from Arabidopsis, digestion, enrichment, and MS analysis of Lys-acetylated peptides are given by Finkemeier et al. (2011).

Statistical Analysis

Unless stated otherwise, results are expressed as means \pm SE of data obtained from independent experiments representing true biological replicates. Significant differences between mean values were calculated using Student's t test.

Preparation of Figures

Fluorescence micrographs including time-lapse movies and z-stacks had within-image annotations (arrows, scale bars, and time stamps) added using Fiji (Schindelin et al., 2012). Occasional additional annotation was performed in Photoshop. All images were exported as TIFFs, and composite figures were constructed in Adobe Illustrator before exporting as TIFFs.

Supplemental Data

The following materials are available in the online version of this article.

Supplemental Figure S1. Analysis of cluster size and number in the *friendly*-3 T-DNA mutant.

Supplemental Figure S2. Disruption of the actin cytoskeleton can phenocopy for *FRIENDLY* mutation while peroxisome distribution is unaffected in *friendly*.

Supplemental Figure S3. Transient expression of *FRIENDLY* N- and C-terminal mRFP1 fusions in *friendly* mutant seedlings.

- Supplemental Figure S4.** Whole plant phenotype of wild type (Col-0) and the *friendly-3* T-DNA mutant.
- Supplemental Figure S5.** Fragmentation spectrum of a lysine-acetylated peptide unique to FRIENDLY (At3g52140).
- Supplemental Table S1.** List of identified significantly regulated nonredundant transcripts.
- Supplemental Movie S1.** Z-stacks through wild type or *friendly* leaves.
- Supplemental Movie S2.** FRAP.
- Supplemental Movie S3.** Mitochondria and actin in the wild type and *friendly*.
- Supplemental Movie S4.** Mitochondrial clusters in the *friendly* mutant are modified by movement through the cytoplasm.
- Supplemental Movie S5.** Mitochondria and actin: development and disruption of a cluster in *friendly*.
- Supplemental Movie S6.** Mitochondrial clusters and microtubules, or the plus-ends of microtubules.
- Supplemental Movie S7.** Dual transient expression of FRIENDLY-GFP and mito-mCherry in a tobacco epidermal cell.
- Supplemental Movie S8.** Mitochondrial association/disassociation events.
- Supplemental Movie S9.** Mitochondrial membrane potential pulsing.
- Supplemental Movie S10.** In vivo fusion assay.
- Supplemental Document S1.** Simple analytic argument recapitulating clustering through modulation of association time.

ACKNOWLEDGMENTS

We thank Barry Martin, Dr. Sarah Irons, and Chris Hawes (all Oxford Brookes University) for high-pressure freezing and microscopy expertise; Dr. Mark D. Fricker (University of Oxford) for providing the software used for the quantitative mEos analysis; the microscopy platform within the Qualité et Santé du Végétal Structure Fédérative de Recherche, IMAC, for support given to the functioning of the Nikon A1 confocal laser-scanning microscope; and Harry Hodge (University of St. Andrews) for excellent technical assistance.

Received May 27, 2014; accepted August 27, 2014; published August 27, 2014.

LITERATURE CITED

- Alexander C, Votruba M, Pesch UEA, Thiselton DL, Mayer S, Moore A, Rodriguez M, Kellner U, Leo-Kottler B, Auburger G, et al (2000) OPA1, encoding a dynamin-related GTPase, is mutated in autosomal dominant optic atrophy linked to chromosome 3q28. *Nat Genet* **26**: 211–215
- Arimura S, Fujimoto M, Doniwa Y, Kadoya N, Nakazono M, Sakamoto W, Tsutsumi N (2008) *Arabidopsis* ELONGATED MITOCHONDRIA1 is required for localization of DYNAMIN-RELATED PROTEIN3A to mitochondrial fission sites. *Plant Cell* **20**: 1555–1566
- Arimura S, Tsutsumi N (2002) A dynamin-like protein (ADL2b), rather than FtsZ, is involved in *Arabidopsis* mitochondrial division. *Proc Natl Acad Sci USA* **99**: 5727–5731
- Arimura S, Yamamoto J, Aida GP, Nakazono M, Tsutsumi N (2004) Frequent fusion and fission of plant mitochondria with unequal nucleoid distribution. *Proc Natl Acad Sci USA* **101**: 7805–7808
- Asada K, Heber U, Schreiber U (1992) Pool size of electrons that can be donated to P700+ as determined in intact leaves: donation to P700+ from stromal components via the intersystem chain. *Plant Cell Physiol* **33**: 927–932
- Aviv D, Galun E (1987) Chondriome analysis in sexual progenies of *Nicotiana* cybrids. *Theor Appl Genet* **73**: 821–826
- Baldi P, Long AD (2001) A Bayesian framework for the analysis of microarray expression data: regularized t-test and statistical inferences of gene changes. *Bioinformatics* **17**: 509–519
- Belliard G, Vedel F, Pelletier G (1979) Mitochondrial recombination in cytoplasmic hybrids of *Nicotiana tabacum* by protoplast fusion. *Nature* **281**: 401–403
- Benamar A, Pierart A, Baecker V, Avelange-Macherel MH, Rolland A, Gaudichon S, Di Gioia L, Macherel D (2013) Simple system using natural mineral water for high-throughput phenotyping of *Arabidopsis thaliana* seedlings in liquid culture. *Int J High Throughput Screen* **4**: 1–15
- Bereiter-Hahn J, Vöth M (1994) Dynamics of mitochondria in living cells: shape changes, dislocations, fusion, and fission of mitochondria. *Microsc Res Tech* **27**: 198–219
- Berry LL, Brzezowski P, Wilson KE (2011) Inactivation of the STT7 gene protects *PsaF*-deficient *Chlamydomonas reinhardtii* cells from oxidative stress under high light. *Physiol Plant* **141**: 188–196
- Boldogh IR, Pon LA (2007) Mitochondria on the move. *Trends Cell Biol* **17**: 502–510
- Brand MD, Nicholls DG (2011) Assessing mitochondrial dysfunction in cells. *Biochem J* **435**: 297–312
- Brandizzi F, Snapp EL, Roberts AG, Lippincott-Schwartz J, Hawes C (2002) Membrane protein transport between the endoplasmic reticulum and the Golgi in tobacco leaves is energy dependent but cytoskeleton independent: evidence from selective photobleaching. *Plant Cell* **14**: 1293–1309
- Bui ET, Bradley PJ, Johnson PJ (1996) A common evolutionary origin for mitochondria and hydrogenosomes. *Proc Natl Acad Sci USA* **93**: 9651–9656
- Candat A, Paszkiewicz G, Neveu M, Gautier R, Logan DC, Avelange-Macherel MH, Macherel D (2014) The ubiquitous distribution of late embryogenesis abundant proteins across cell compartments in *Arabidopsis* offers tailored protection against abiotic stress. *Plant Cell* **26**: 3148–3166
- Chen H, Chan DC (2009) Mitochondrial dynamics—fusion, fission, movement, and mitophagy—in neurodegenerative diseases. *Hum Mol Genet* **18**: R169–R176
- Chen YN, Slabaugh E, Brandizzi F (2008) Membrane-tethered transcription factors in *Arabidopsis thaliana*: novel regulators in stress response and development. *Curr Opin Plant Biol* **11**: 695–701
- Clark CG, Roger AJ (1995) Direct evidence for secondary loss of mitochondria in *Entamoeba histolytica*. *Proc Natl Acad Sci USA* **92**: 6518–6521
- Clough SJ, Bent AF (1998) Floral dip: a simplified method for *Agrobacterium*-mediated transformation of *Arabidopsis thaliana*. *Plant J* **16**: 735–743
- Cox RT, Spradling AC (2009) Clueless, a conserved *Drosophila* gene required for mitochondrial subcellular localization, interacts genetically with parkin. *Dis Model Mech* **2**: 490–499
- Curtis MD, Grossniklaus U (2003) A Gateway cloning vector set for high-throughput functional analysis of genes in planta. *Plant Physiol* **133**: 462–469
- De Clercq I, Vermeirssen V, Van Aken O, Vandepoele K, Murcha MW, Law SR, Inzé A, Ng S, Ivanova A, Rombaut D, et al (2013) The membrane-bound NAC transcription factor ANAC013 functions in mitochondrial retrograde regulation of the oxidative stress response in *Arabidopsis*. *Plant Cell* **25**: 3472–3490
- Delettre C, Lenaers G, Griffoin JM, Gignarel N, Lorenzo C, Belenguer P, Pelloquin L, Grosgeorge J, Turc-Carel C, Perret E, et al (2000) Nuclear gene OPA1, encoding a mitochondrial dynamin-related protein, is mutated in dominant optic atrophy. *Nat Genet* **26**: 207–210
- Douzery EJP, Snell EA, Baptiste E, Delsuc F, Philippe H (2004) The timing of eukaryotic evolution: does a relaxed molecular clock reconcile proteins and fossils? *Proc Natl Acad Sci USA* **101**: 15386–15391
- Ekanayake DSB, El Zawily AM, Logan DC (2014) Visualising and quantifying plant mitochondrial dynamics. *Methods Mol Biol* (in press)
- Feldmann KA, Malmberg RL, Dean C (1994) Mutagenesis in *Arabidopsis*. In EM Meyerowitz, CR Somerville, eds, *Arabidopsis*. Cold Spring Harbor Laboratory Press, Cold Spring Harbor, NY, pp 137–172
- Feng DF, Cho G, Doolittle RF (1997) Determining divergence times with a protein clock: update and reevaluation. *Proc Natl Acad Sci USA* **94**: 13028–13033
- Fields SD, Arana Q, Heuser J, Clarke M (2002) Mitochondrial membrane dynamics are altered in *cluA*- mutants of *Dictyostelium*. *J Muscle Res Cell Motil* **23**: 829–838
- Finkemeier I, Laxa M, Miguet L, Howden AJM, Sweetlove LJ (2011) Proteins of diverse function and subcellular location are lysine acetylated in *Arabidopsis*. *Plant Physiol* **155**: 1779–1790
- Frederick RL, Shaw JM (2007) Moving mitochondria: establishing distribution of an essential organelle. *Traffic* **8**: 1668–1675
- Gao C, Xing D, Li L, Zhang L (2008) Implication of reactive oxygen species and mitochondrial dysfunction in the early stages of plant programmed cell death induced by ultraviolet-C overexposure. *Planta* **227**: 755–767

- Garçon C, Baltensperger R, Fournier T, Pasquier J, Schnetzer MA, Gabriel JP, Métraux JP** (2006) FiRe and microarrays: a fast answer to burning questions. *Trends Plant Sci* **11**: 320–322
- Genty B, Harbinson J, Briantais JM, Baker NR** (1990) The relationship between non-photochemical quenching of chlorophyll fluorescence and the rate of photosystem 2 photochemistry in leaves. *Photosynth Res* **25**: 249–257
- Gillespie DT** (1977) Exact stochastic simulation of coupled chemical-reactions. *J Phys Chem* **81**: 2340–2361
- Gray MW, Burger G, Lang BF** (1999) Mitochondrial evolution. *Science* **283**: 1476–1481
- Hedges SB, Blair JE, Venturi ML, Shoe JL** (2004) A molecular timescale of eukaryote evolution and the rise of complex multicellular life. *BMC Evol Biol* **4**: 2
- Hoppins S, Nunnari J** (2009) The molecular mechanism of mitochondrial fusion. *Biochim Biophys Acta* **1793**: 20–26
- Huang X, Sun L, Ji S, Zhao T, Zhang W, Xu J, Zhang J, Wang Y, Wang X, Franzini-Armstrong C, et al** (2013) Kissing and nanotunneling mediate intermitochondrial communication in the heart. *Proc Natl Acad Sci USA* **110**: 2846–2851
- Ito J, Bathth TS, Petzold CJ, Redding-Johanson AM, Mukhopadhyay A, Verboom R, Meyer EH, Millar AH, Heazlewood JL** (2011) Analysis of the Arabidopsis cytosolic proteome highlights subcellular partitioning of central plant metabolism. *J Proteome Res* **10**: 1571–1582
- Ivanov AG, Morgan RM, Gray GR, Velitchkova MY, Huner NP** (1998) Temperature/light dependent development of selective resistance to photoinhibition of photosystem I. *FEBS Lett* **430**: 288–292
- Karbowski M, Youle RJ** (2003) Dynamics of mitochondrial morphology in healthy cells and during apoptosis. *Cell Death Differ* **10**: 870–880
- Kost B, Spielhofer P, Chua NH** (1998) A GFP-mouse talin fusion protein labels plant actin filaments in vivo and visualizes the actin cytoskeleton in growing pollen tubes. *Plant J* **16**: 393–401
- Kramer DM, Johnson G, Kiirats O, Edwards GE** (2004) New fluorescence parameters for the determination of q(a) redox state and excitation energy fluxes. *Photosynth Res* **79**: 209–218
- Krause GH, Weis E** (1991) Chlorophyll fluorescence and photosynthesis: the basics. *Annu Rev Plant Physiol Plant Mol Biol* **42**: 313–349
- Kumar A, Agarwal S, Heyman JA, Matson S, Heidtman M, Piccirillo S, Umansky L, Drawid A, Jansen R, Liu Y, et al** (2002) Subcellular localization of the yeast proteome. *Genes Dev* **16**: 707–719
- Liu Y, Samuel BS, Breen PC, Ruvkun G** (2014) Caenorhabditis elegans pathways that surveil and defend mitochondria. *Nature* **508**: 406–410
- Logan DC** (2003) Mitochondrial dynamics. *New Phytol* **160**: 463–478
- Logan DC** (2006) The mitochondrial compartment. *J Exp Bot* **57**: 1225–1243
- Logan DC** (2010a) The dynamic plant chondriome. *Semin Cell Dev Biol* **21**: 550–557
- Logan DC** (2010b) Mitochondrial fusion, division and positioning in plants. *Biochem Soc Trans* **38**: 789–795
- Logan DC, Leaver CJ** (2000) Mitochondria-targeted GFP highlights the heterogeneity of mitochondrial shape, size and movement within living plant cells. *J Exp Bot* **51**: 865–871
- Logan DC, Scott I, Tobin AK** (2003) The genetic control of plant mitochondrial morphology and dynamics. *Plant J* **36**: 500–509
- Logan DC, Scott I, Tobin AK** (2004) ADL2a, like ADL2b, is involved in the control of higher plant mitochondrial morphology. *J Exp Bot* **55**: 783–785
- Lonsdale DM, Brears T, Hodge TP, Melville SE, Rottmann WH** (1988) The plant mitochondrial genome: homologous recombination as a mechanism for generating heterogeneity. *Philos Trans R Soc Lond B Biol Sci* **319**: 149–163
- Mano S, Nakamori C, Hayashi M, Kato A, Kondo M, Nishimura M** (2002) Distribution and characterization of peroxisomes in Arabidopsis by visualization with GFP: dynamic morphology and actin-dependent movement. *Plant Cell Physiol* **43**: 331–341
- Mathur J, Chua NH** (2000) Microtubule stabilization leads to growth reorientation in Arabidopsis trichomes. *Plant Cell* **12**: 465–477
- Mathur J, Mathur N, Hülskamp M** (2002) Simultaneous visualization of peroxisomes and cytoskeletal elements reveals actin and not microtubule-based peroxisome motility in plants. *Plant Physiol* **128**: 1031–1045
- Mathur J, Mathur N, Kernebeck B, Srinivas BP, Hülskamp M** (2003) A novel localization pattern for an EB1-like protein links microtubule dynamics to endomembrane organization. *Curr Biol* **13**: 1991–1997
- Mathur J, Radhamony R, Sinclair AM, Donoso A, Dunn N, Roach E, Radford D, Mohaghegh PSM, Logan DC, Kokolic K, et al** (2010) mEosFP-based green-to-red photoconvertible subcellular probes for plants. *Plant Physiol* **154**: 1573–1587
- Meyerowitz EM, Somerville CR, editors** (1994) Arabidopsis. Cold Spring Harbor Laboratory Press, Cold Spring Harbor, NY
- Moran R** (1982) Formulae for determination of chlorophyllous pigments extracted with N,N-dimethylformamide. *Plant Physiol* **69**: 1376–1381
- Nakashima K, Takasaki H, Mizoi J, Shinozaki K, Yamaguchi-Shinozaki K** (2012) NAC transcription factors in plant abiotic stress responses. *Biochim Biophys Acta* **1819**: 97–103
- Nebenführ A, Gallagher LA, Dunahay TG, Frohlich JA, Mazurkiewicz AM, Meehl JB, Staehelin LA** (1999) Stop-and-go movements of plant Golgi stacks are mediated by the acto-myosin system. *Plant Physiol* **121**: 1127–1142
- Nelson BK, Cai X, Nebenführ A** (2007) A multicolored set of in vivo organelle markers for co-localization studies in Arabidopsis and other plants. *Plant J* **51**: 1126–1136
- Ng S, Ivanova A, Duncan O, Law SR, Van Aken O, De Clercq I, Wang Y, Carrie C, Xu L, Kmiec B, et al** (2013) A membrane-bound NAC transcription factor, ANAC017, mediates mitochondrial retrograde signaling in Arabidopsis. *Plant Cell* **25**: 3450–3471
- Nunnari J, Suomalainen A** (2012) Mitochondria: in sickness and in health. *Cell* **148**: 1145–1159
- Okamoto K, Shaw JM** (2005) Mitochondrial morphology and dynamics in yeast and multicellular eukaryotes. *Annu Rev Genet* **39**: 503–536
- Olson KR, McIntosh JR, Olmsted JB** (1995) Analysis of MAP 4 function in living cells using green fluorescent protein (GFP) chimeras. *J Cell Biol* **130**: 639–650
- Osterrieder A, Hummel E, Carvalho CM, Hawes C** (2010) Golgi membrane dynamics after induction of a dominant-negative mutant Sar1 GTPase in tobacco. *J Exp Bot* **61**: 405–422
- Rafelski SM** (2013) Mitochondrial network morphology: building an integrative, geometrical view. *BMC Biol* **11**: 71
- Rice DW, Alverson AJ, Richardson AO, Young GJ, Sanchez-Puerta MV, Munzinger J, Barry K, Boore JL, Zhang Y, dePamphilis CW, et al** (2013) Horizontal transfer of entire genomes via mitochondrial fusion in the angiosperm Amborella. *Science* **342**: 1468–1473
- Runkel ED, Liu S, Baumeister R, Schulze E** (2013) Surveillance-activated defenses block the ROS-induced mitochondrial unfolded protein response. *PLoS Genet* **9**: e1003346
- Sampathkumar A, Lindeboom JJ, Debolt S, Gutierrez R, Ehrhardt DW, Ketelaar T, Persson S** (2011) Live cell imaging reveals structural associations between the actin and microtubule cytoskeleton in Arabidopsis. *Plant Cell* **23**: 2302–2313
- Santo-Domingo J, Giacomello M, Poburko D, Scorrano L, Demareux N** (2013) OPA1 promotes pH flashes that spread between contiguous mitochondria without matrix protein exchange. *EMBO J* **32**: 1927–1940
- Schindelin J, Arganda-Carreras I, Frise E, Kaynig V, Longair M, Pietzsch T, Preibisch S, Rueden C, Saalfeld S, Schmid B, et al** (2012) Fiji: an open-source platform for biological-image analysis. *Nat Methods* **9**: 676–682
- Schreiber U, Klughammer C, Neubauer C** (1988) Measuring P700 absorbance changes around 830 nm with a new type of pulse modulation system. *Z Naturforsch* **43c**: 686–698
- Schwarzländer M, König AC, Sweetlove LJ, Finkemeier I** (2012a) The impact of impaired mitochondrial function on retrograde signalling: a meta-analysis of transcriptomic responses. *J Exp Bot* **63**: 1735–1750
- Schwarzländer M, Logan DC, Johnston IG, Jones NS, Meyer AJ, Fricker MD, Sweetlove LJ** (2012b) Pulsing of membrane potential in individual mitochondria: a stress-induced mechanism to regulate respiratory bioenergetics in Arabidopsis. *Plant Cell* **24**: 1188–1201
- Scott I, Logan DC** (2008) Mitochondrial morphology transition is an early indicator of subsequent cell death in Arabidopsis. *New Phytol* **177**: 90–101
- Scott I, Tobin AK, Logan DC** (2006) BIGYIN, an orthologue of human and yeast FIS1 genes functions in the control of mitochondrial size and number in Arabidopsis thaliana. *J Exp Bot* **57**: 1275–1280
- Sen A, Damm VT, Cox RT** (2013) Drosophila clueless is highly expressed in larval neuroblasts, affects mitochondrial localization and suppresses mitochondrial oxidative damage. *PLoS ONE* **8**: e54283
- Shaner NC, Campbell RE, Steinbach PA, Giepmans BNG, Palmer AE, Tsien RY** (2004) Improved monomeric red, orange and yellow fluorescent proteins derived from Discosoma sp. red fluorescent protein. *Nat Biotechnol* **22**: 1567–1572
- Shaw JM, Nunnari J** (2002) Mitochondrial dynamics and division in budding yeast. *Trends Cell Biol* **12**: 178–184

- Shutt TE, McBride HM** (2013) Staying cool in difficult times: mitochondrial dynamics, quality control and the stress response. *Biochim Biophys Acta* **1833**: 417–424
- Sparkes IA, Runions J, Kearns A, Hawes C** (2006) Rapid, transient expression of fluorescent fusion proteins in tobacco plants and generation of stably transformed plants. *Nat Protoc* **1**: 2019–2025
- Sparkes IA, Teanby NA, Hawes C** (2008) Truncated myosin XI tail fusions inhibit peroxisome, Golgi, and mitochondrial movement in tobacco leaf epidermal cells: a genetic tool for the next generation. *J Exp Bot* **59**: 2499–2512
- Teh OK, Moore I** (2007) An ARF-GEF acting at the Golgi and in selective endocytosis in polarized plant cells. *Nature* **448**: 493–496
- Thimm O, Bläsing O, Gibon Y, Nagel A, Meyer S, Krüger P, Selbig J, Müller LA, Rhee SY, Stitt M** (2004) MAPMAN: a user-driven tool to display genomics data sets onto diagrams of metabolic pathways and other biological processes. *Plant J* **37**: 914–939
- Tran LSP, Nakashima K, Sakuma Y, Simpson SD, Fujita Y, Maruyama K, Fujita M, Seki M, Shinozaki K, Yamaguchi-Shinozaki K** (2004) Isolation and functional analysis of *Arabidopsis* stress-inducible NAC transcription factors that bind to a drought-responsive *cis*-element in the *early responsive to dehydration stress 1* promoter. *Plant Cell* **16**: 2481–2498
- Tse YC, Lo SW, Hillmer S, Dupree P, Jiang L** (2006) Dynamic response of prevacuolar compartments to brefeldin A in plant cells. *Plant Physiol* **142**: 1442–1459
- Twig G, Elorza A, Molina AJA, Mohamed H, Wikstrom JD, Walzer G, Stiles L, Haigh SE, Katz S, Las G, et al** (2008) Fission and selective fusion govern mitochondrial segregation and elimination by autophagy. *EMBO J* **27**: 433–446
- Usadel B, Nagel A, Thimm O, Redestig H, Blaessing OE, Palacios-Rojas N, Selbig J, Hannemann J, Piques MC, Steinhauser D, et al** (2005) Extension of the visualization tool MapMan to allow statistical analysis of arrays, display of corresponding genes, and comparison with known responses. *Plant Physiol* **138**: 1195–1204
- van Kooten O, Snel JFH** (1990) The use of chlorophyll fluorescence nomenclature in plant stress physiology. *Photosynth Res* **25**: 147–150
- Vellosillo T, Aguilera V, Marcos R, Bartsch M, Vicente J, Cascón T, Hamberg M, Castresana C** (2013) Defense activated by 9-lipoxygenase-derived oxylipins requires specific mitochondrial proteins. *Plant Physiol* **161**: 617–627
- Vicente JA, Peixoto F, Lopes ML, Madeira VM** (2001) Differential sensitivities of plant and animal mitochondria to the herbicide paraquat. *J Biochem Mol Toxicol* **15**: 322–330
- Xiang D, Venglat P, Tibiche C, Yang H, Risseuw E, Cao Y, Babic V, Cloutier M, Keller W, Wang E, et al** (2011) Genome-wide analysis reveals gene expression and metabolic network dynamics during embryo development in *Arabidopsis*. *Plant Physiol* **156**: 346–356
- Yoshimoto K** (2012) Beginning to understand autophagy, an intracellular self-degradation system in plants. *Plant Cell Physiol* **53**: 1355–1365
- Zhang L, Xing D** (2008) Methyl jasmonate induces production of reactive oxygen species and alterations in mitochondrial dynamics that precede photosynthetic dysfunction and subsequent cell death. *Plant Cell Physiol* **49**: 1092–1111
- Zhu Q, Hulen D, Liu T, Clarke M** (1997) The *cluA*-mutant of *Dictyostelium* identifies a novel class of proteins required for dispersion of mitochondria. *Proc Natl Acad Sci USA* **94**: 7308–7313